Printable, Stretchable Liquid Metal Conductors Based on EGaIn-Ecoflex Composites

Ren-Mian Chin

A thesis

submitted in partial fulfillment of

the requirements for the degree of

Master of Science

University of Washington

2023

Committee:

Mohammad H. Malakooti

Miqin Zhang

Program Authorized to Offer Degree:

Department of Materials Science and Engineering

University of Washington

Abstract

Printable, Superstretchable Strain-Activated Liquid Metal Conductors Based on EGaIn-Ecoflex Composites

Ren-Mian Chin

Chair of the Supervisory Committee:
Mohammad H. Malakooti
Department of Materials Science and Engineering

Liquid metal elastomer composite (LMEC) brings unique advantages for soft and stretchable electronics by patterning flexible electrical circuitry. By incorporating 3D printing technology, seamless design configuration with high manufacturability of stretchable electronics can be achieved. However, the option of elastomers is greatly limited by the immediate surface oxidation of liquid metal (LM) particles. When we try to increase the stretchability of liquid metal elastomer composite (LMEC) by using ultra-soft elastomers, the failure to conduct electricity often occurs. In addition, tiny LM particles (1-5 microns) have better printing performance and also cause LMEC not to be conductive. Therefore, it is extremely challenging to use both highly stretchable soft elastomers (such as Ecoflex 00-30) and small-sized LM particles to make stretchable conductors.

In this study, we address three key scientific questions about liquid metal composites and their electromechanical response. Firstly, we investigate the successful synthesis of conductive LMEC

from highly stretchable silicone elastomers with particle sizes approaching 1 micron. Secondly, we examine whether the LM microparticles experience an increase in size when dispersed in an elastomer. Lastly, we explore the relationship between the electromechanical response of LM-based conductors and the rate of applied deformation. These questions and hypotheses serve as the foundation for our research and provide valuable insights into the behavior of LMEC in various conditions. The results show the printed composites show excellent electrical and electromechanical properties, such as an electrical resistance of 0.2 Ω/cm at unload, a low resistance variation up to 700% uniaxial tensile strain. The robustness of LMEC was also tested for 1000 cycles at 300% uniaxial tensile strain and 5000 cycles at 200% uniaxial tensile strain. Additionally, the LMEC exhibited an extremely low resistance variation even under high-speed displacement, highlighting its potential for applications in stretchable and wearable electronics. These findings highlights the promising capabilities of LMEC in various practical applications.

Acknowledgements

In a blink of an eye, I have been in the iMatter Lab for over a year. Originally, I only planned to practice my English by joining the lab, but I ended up spending more and more time in the lab and eventually changed it to a thesis graduation option.

I am very grateful to my advisor, Prof. Mohammad H. Malakooti, who really took a lot of time to help me adjust to the pace of research in the United States. Many of the individual discussions were enlightening and saved me a lot of time. I have never met a professor who was willing to spend so much time with a student, including my graduation defense, where he spent hours discussing and revising the slides with me. He set a very good model, teaching me how to question things and how to solve problems. I can say that my time in graduate school at the University of Washington was the fastest learning period for me. Also, I felt my passion for experimentation and developed the idea of pursuing a PhD, all of which happened in just one year. Once again, I would like to thank my advisor, Prof. Mohammad H. Malakooti, without whose help this thesis would never have been possible.

Thanks to my parents, it was a great decision for me to come to UW and it was only because of their support that I was able to make it this far. I am very happy to have parents who are open-minded and supportive of many of my decisions. I think I owe my healthy personality traits to their influence. Every Friday night video family gathering is full of fun and is the time I cherish the most. I am going to continue my doctoral studies and hope to help them in the near future.

Thanks to Young, I would never have progressed in many of my experiments without his help, and he has provided many valuable suggestions and ideas. His wealth of knowledge has always inspired me, and I have learned something new from it. I thank him for his help and look forward to working with him in the future.

Thanks to Natee and Lijun, who chatted with me and solved some experimental problems while doing the experiment. The time I spent with you in the lab made me feel that doing experiments is not boring, but very happy.

Thanks to Halil and Cerwyn, you provided me with a lot of professional knowledge about experimental software, reports and presentations, and showed me what a good report is, which made me gain a lot.

Thanks to my girlfriend Doris for listening to me complain about my failed experiments and talking about a bunch of terms I don't understand. It is really important to have someone who listens to you.

Thanks to Andy for talking to me so often and answering so many of questions. I can say that you were definitely the one who pushed me to make my decision to study for my PhD.

Thank you to the other people I didn't mention, too many people I often chat with I can't say my thanks in accordance, If I often chat with you, it may mean that I and you are very leisurely, or I think it is very pleasant to chat with you. Thank you all!

Table of Contents

Table of images

List of Acronyms

Acronym	Full meaning
1.3M	1,300,000
AI	Artificial Intelligence
DLS	Dynamic Light Scattering
EGaIn	Eutectic Gallium-indium
GaInAs	Gallium Indium Arsenide
GaInAsP	Gallium Indium Arsenide Phosphide
IPA	Isopropyl Alcohol
LED	Light-emitting Diode
LM	Liquid Metal
LMEC	Liquid Metal Elastomer Composite
MPa	Mega Pascal
MW	Molecular Weight
OM	Optical Microscope
PCB	Printed Circuit Board
PDMS	Polydimethylsiloxane
PVP	Polyvinylpyrrolidone
P&D	Power and Duration of ultrasonic coefficients
R	Electrical Resistance
R_0	Initial Electrical Resistance
rpm	Revolutions Per Minute
(S)	Shear Mixing
SEM	Scanning Electron Microscopy
wt.%	Weight Percentage
ΔR	Resistance Variation

1. Introduction

1.1. Review of Stretchable Electronics

Stretchable electronics have the potential to transform the world of electronics by providing a new class of devices with distinct mechanical features due to their outstanding mechanical and electrical qualities, such as high stretchability, flexibility, conformability, and resilience. These interesting properties make them perfect for a variety of applications such as batteries,[1,2] electronic skin,[3,4] electronic implants,[5,6] and generators.[7–9] The development of dependable and scalable manufacturing processes for mass production is one of the primary research priorities in the field of stretchable electronics. Stretchable electronics production is far more sophisticated than standard electronic devices such as printed circuit boards (PCBs) and is heavily impacted by the selection of suitable materials. Because of the wide-ranging possibilities afforded by mixing filled materials with flexible polymers, conductive composites have emerged as a very attractive research topic for stretchy electronics. A variety of filler materials, including as silver nanowires,[10] carbon nanotubes,[4] and micro/nanoparticles,[11,12] are being investigated, as well as a wide range of flexible polymers, such as polymeric organosilicon compounds,[13,14] thermoplastic elastomers,[15] and other polymers.[16–18] The introduction of conductive composites has substantially improved the performance of stretchable electronics, allowing for high electrical conductivity while supporting good stretchability of more than 100% strain. The combination of favorable material qualities and a wide range of options makes conductive composites extremely adaptable for use in a variety of applications, including the biomedical industry.[19–21] Despite the obvious benefits of conductive composites, stretchy electronics face a number of obstacles. These difficulties include concerns such as the sophisticated fabrication process, which prevents large-scale manufacture, the vulnerability to instability over time, and the need to increase stretchability to broaden the spectrum of potential uses.

1.2. Review of Liquid Metals

Gallium liquid metal (LM) alloys, such as eutectic gallium-indium (EGaIn), have several desired qualities, including low toxicity,[22] high electrical conductivity (3.4×10^6 S m^{-1}),[23] and exceptional deformability, thereby making it an excellent candidate for stretchable electronics. and extraordinary deformability, making it a good choice for flexible electronics. Furthermore, its capacity to self-heal and adjust to variable surface topography gives it a competitive advantage over other materials in the area, with applications ranging from soft robotics to wearable sensors.

Depending on the application, direct deposition of EGaIn onto a substrate can be accomplished by syringe dispensing,[9,13] microfluidics,[24,25] or stencil printing.[26,27] Alternatively, liquid metal embedded elastomers (LMEC), which are stretchable composites that maintain electrical conductivity and adapt to complicated surfaces, can be created by embedding EGaIn within elastomeric matrices like PDMS.[9,13,14] The high surface tension of bulk LM makes it difficult to fabricate high-resolution designs, making printing methods impractical. Contrarily, LMEC offers intriguing opportunities for the creation of printing circuits by enhancing printability while also enhancing the material's stretchability and other mechanical qualities.[15–18] The existence of oxide shells, which prevent charge conduction between nearby particles, makes the layers of EGaIn particles in the elastomer matrix from being conductive when they are printed. To get around this restriction, the oxide shell of the EGaIn must be ruptured under severe mechanical stress, which interferes with the electrical connection.[28–31] This leads to the creation of continuous charge conduction pathways. There have been reports of theoretical yield stresses of over 1 and 10 MPa for micron- and nano-sized EGaIn particles, respectively.[28,29] Recently, a promising new method that achieves the same electrical conductivity without suffering mechanical damage has been created utilizing strain-activated LMEC, displaying remarkable efficiency and durability.[13,32,33] In the current work, the electrical conductivity of LMEC functionalized with polyvinylpyrrolidone (PVP) is examined using polydimethylsiloxane (PDMS) as the elastomer matrix. These composites have a phenomenal electrical conductivity of 8000 S/cm when stretched.[13] However, because PDMS is a rigid elastomer with limited stretchability, its range of use is only around 100% strain.[14,26] Stretchability has become a crucial measure in the development of stretchable electronics. Therefore, it is crucial to find methods that can increase stretchability while maintaining the effectiveness of strain-activation.

1.3. Hypothesis: Strain-activation Using Soft Elastomers

Soft elastomers, sometimes called low elastic modulus elastomers, are more stretchable and flexible than stiff elastomers. These elastomers have become more well-known recently due to their exceptional qualities.[34–36] The research community holds Ecoflex rubbers in high value as soft elastomers because of their quick and easy synthetic construction and exceptional stretchability at about 900% strain.[34,36,37] It is difficult to use soft elastomers for strain-activated LMEC because of their low elastic modulus, which prevents them from applying enough shear stress to crack the oxide shell. With a focus on surface modification of the oxide shell, weakening

the solid-liquid interface of EGaIn particles is thus demonstrated. Polymer packaging has been suggested as a viable remedy to achieve this. The results of the study suggest that PVP has the capacity to improve the binding with the elastomer matrix.[13] The solid-liquid interface can become weaker and a continuous conducting pathway can emerge as a result of the strong binding, which can considerably increase the shear stress and cause the oxide shell to break during the strain.

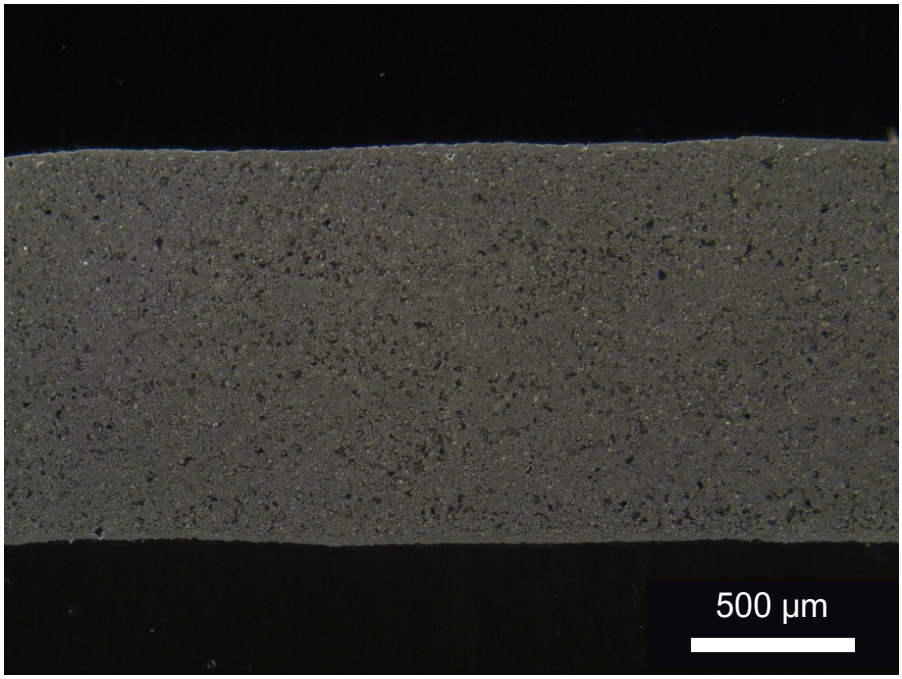

Figure 1 The micrograph of a printing pathway of LMEC

1.4. Terminology

1.4.1. Activation

When EGaIn undergoes sonication to reduce its particle size, EGaIn will oxidize to form an oxide shell, Ga_2O_3/Ga^{3+}.[38] At this time, although EGaIn particles can form a conductive pathway through the contact of the oxide shell, the efficiency is not good. Therefore, breaking the oxide shell to make the liquid EGaIn percolate (flow out) to form a more effective conductive pathway is the first choice. Mechanical stress, such as pressing, is required to rupture the oxide shell, this action is called “activation”. A sample is considered activated when a resistance is detected, and not activated when no resistance is detected.

In this work, we introduced strain-activation as a recently popular method of activation. Since all stretchable circuits will be stretched, strain-activation will be automatically processed during the

first several strains. It has many advantages, such as no damage to the circuit, high efficiency, etc. It is expected to become the mainstream activation method of EGaIn in the future.

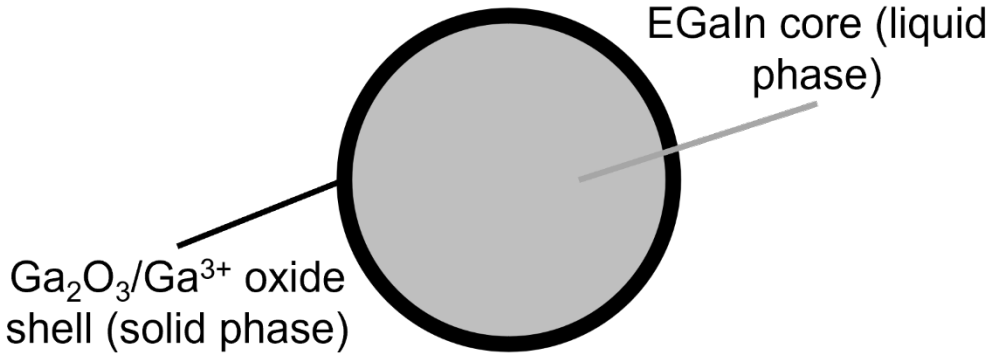

Figure 2 Illustration of EGaIn particle with oxide shell

1.4.2. Elastomer

A polymer substance known as an elastomer has characteristics similar to those of rubber, such as great elasticity, flexibility, and deformability. Examples of elastomers include natural rubber, synthetic rubber, silicone rubber (PDMS and Ecoflex), and polyurethane rubber. Elastomers are frequently utilized in a variety of applications, such as tires, gaskets, seals, and shock absorbers, due to their superior mechanical characteristics and resistance to wear, abrasion, and fatigue. Because of their biocompatibility and low toxicity, they are also employed in medical equipment including gloves and tubing.

1.4.3. Precursor

A precursor is a substance or compound that is utilized to begin the synthesis or creation of another component or material. It is subjected to chemical reactions or transformations in order to produce the desired final product. For the regulated creation of complex chemicals, precursors are significant in domains such as chemistry, materials science, and medicines.

In this work, both synthetic units A&B are precursors.

1.4.4. Pouillet's Law

Pouillet's Law, also known as the electrical resistivity equation, is named after French scientist Claude Pouillet, who initially put out the law in the middle of the 19th century. The equation can be written as:

$$R = (\rho * L) / A$$

where R is the electrical resistance of the material, ρ is the electrical resistivity of the material, L is the length of the material, and A is the cross-sectional area of the material.

When we measure the electromechanical properties, the length (L) and cross-sectional area (A) change as the material is deformed by stretching. Therefore, Poillet's law can be used to predict the change in resistance of a material (R) after stretching in an ideal condition.

1.4.5. Resistance variation

Resistance variation, also known as normalized resistance change, is a popular method to show changes in electrical conductivity. The equation can be written as:

$$\text{Resistance variation} = (R - R_0) / R_0 * 100 \text{ or } \Delta R / R_0 * 100$$

Where R is the current electrical resistance of the material and R_0 is the initial electrical resistance after activation of the material. The unit of resistance variation is percentage (%).

1.4.6. Sonication

Sonication refers to the process of applying high-frequency sound waves (more than 20 kHz) to a substance, typically in a liquid medium. These high-frequency sound waves cause the liquid to undergo alternate cycles of compression and rarefaction, resulting in cavitation bubbles, which are tiny vacuum bubbles or voids. The cavitation bubbles are created during the compression phase, and once the rarefaction phase begins, they quickly implode or collapse. These bubbles' collapse creates agitation and microstreaming in the liquid by producing strong local forces and high temperatures. Then, these forces can decrease the particle size of EGaIn and disperse them uniformly in a liquid medium.

2. Backgrounds

Wearable devices are very close to people's daily life, including headphones and watch accessories are all wearable electronics. In recent years, more and more wearable devices have been invented and have greatly changed our lives. From virtual reality headgear to smart glasses, to Apple's new smart eye wear (Vision Pro), there is no doubt that this will be the trend of our future society: smaller devices worn on the human body.

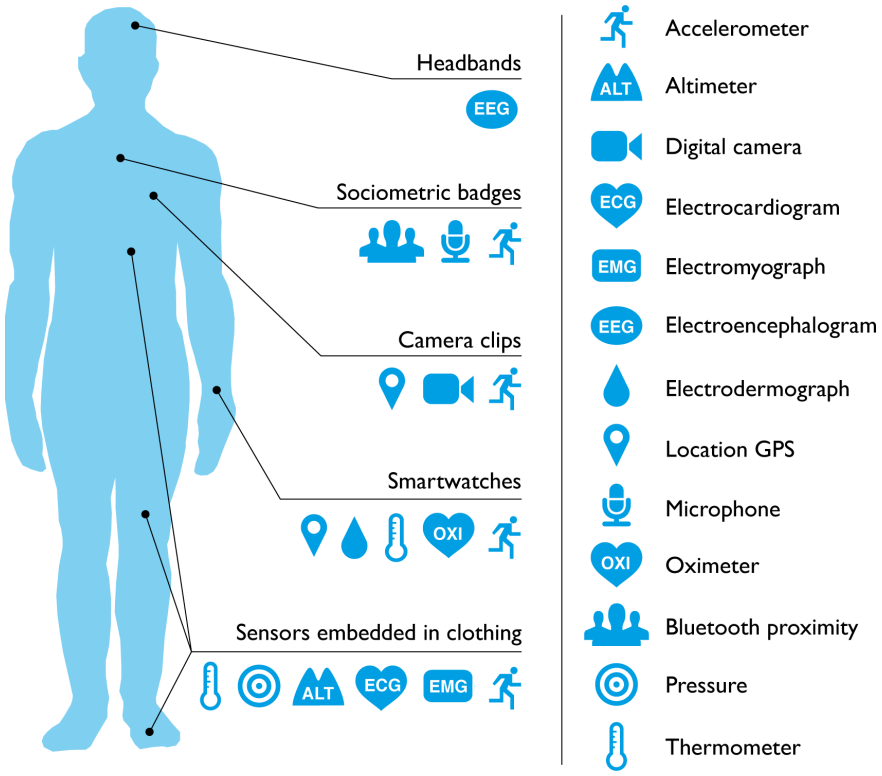

Figure 3 Consumer health wearables, including sensors needed for different body parts. Reprinted with permission from Piwek et al.[39] Copyright 2016, PLOS Medicine

Stretchable electronics is a future star in an application field that is brimming with opportunities. Previously, most wearable devices could be called excellent by simply being bendable and twistable. However, our human body is so mobile that flexibility is not enough for all applications. This is the origin of stretchable devices and stretchable electronics, which not only surpass ordinary wearable devices in terms of flexibility, but also have the potential of ultra-high pulling depth, which can completely match the human body's joint movement to make previously unexpected devices.

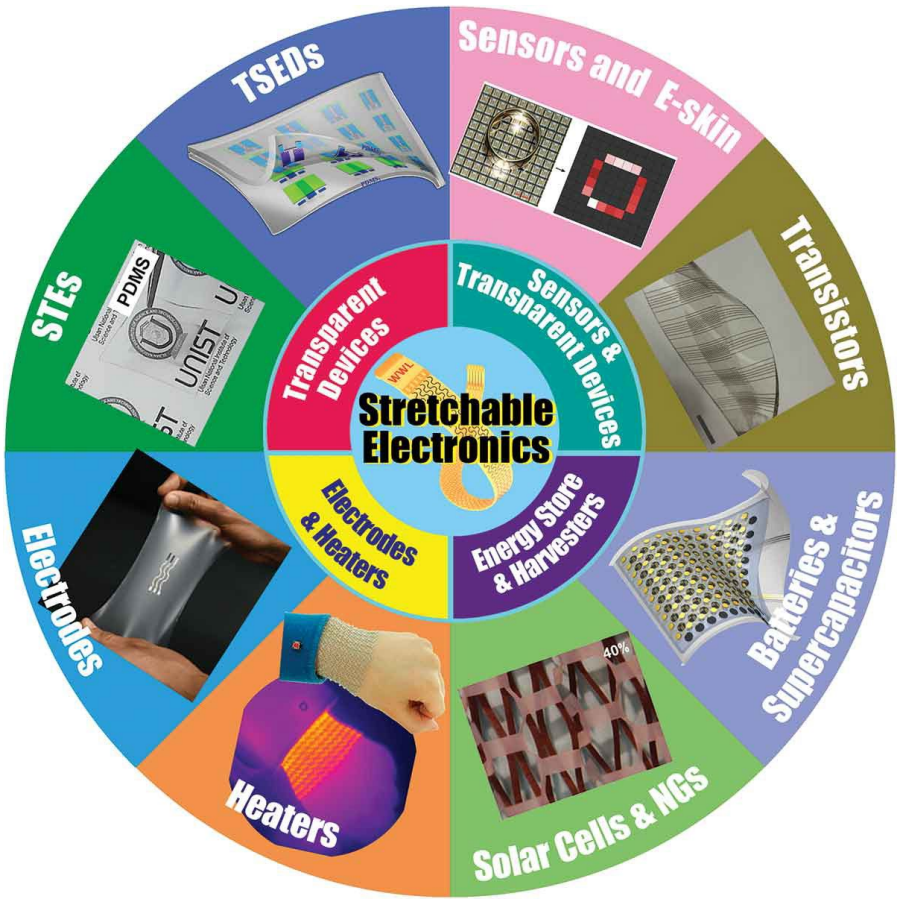

Figure 4 Stretchable electronics for a wide range of applications. Reprinted with permission from Wu et al.[40] Copyright 2019, Science and Technology of Advanced Materials

It is not easy to make stretchable electrons with high stretchability and electrical conductivity, but liquid metals are a good option. Of course, pure liquid metals do not have stretchability, but the incentives such as high electrical conductivity and easy fabrication still attract researchers to improve them. In addition to front-end studies that directly change the material phase of liquid metals,[38,41] liquid metal elastomer composites (LMEC) have high potential because of the freedom to mix and match the constituent materials to obtain desired properties.[42–44] More importantly, the excellent thermal and electrical conductivity of liquid metals combined with the high stretchability of elastomers makes the future of stretchable electronics very promising.

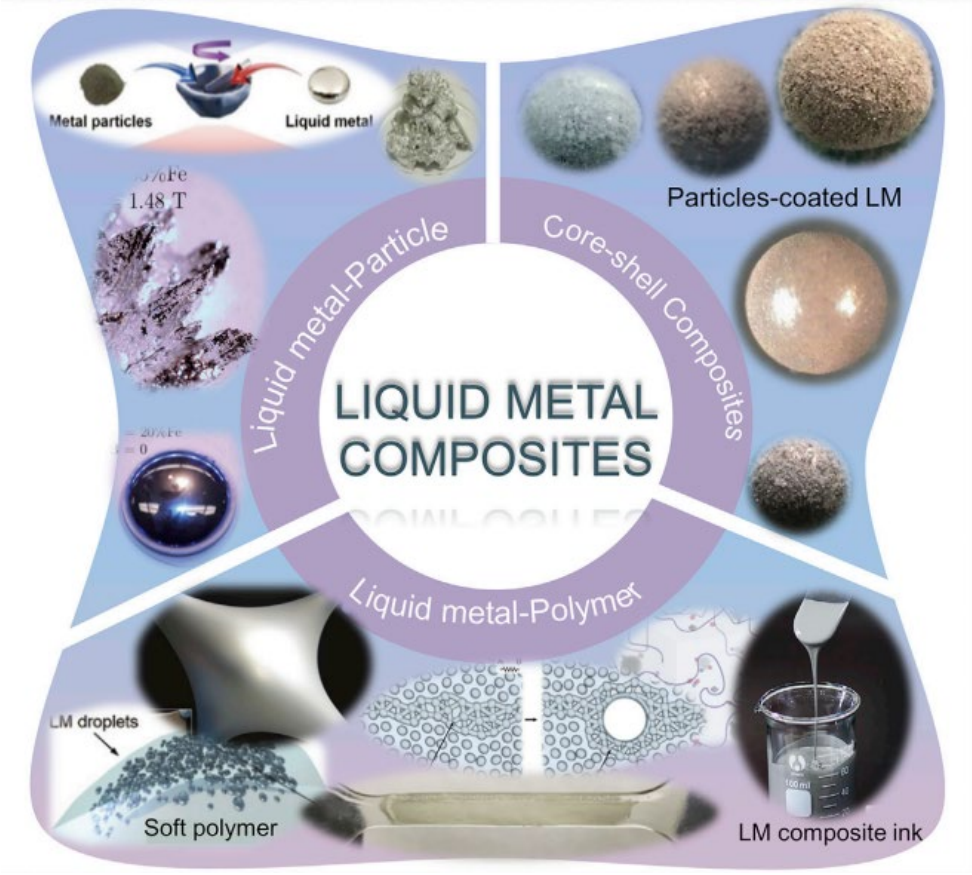

Figure 5 Different types of liquid metal composites, such as liquid metal-particle, liquid metal-polymer, and core-shell composites. Reprinted with permission from Chen et al.[45] Copyright 2020, Matter

However, while the combinations of LMECs may seem to vary widely, the selection of elastomers is actually difficult to go beyond a few specific elastomers because the liquid metal particles need to be activated to form a conductive pathway, which greatly limits the options of elastomers. First of all, activation is the primary difficulty in making LMEC because without activation, the material is not conductive. Activation means that the liquid metal, such as eutectic gallium-indium (EGaIn), will naturally form a gallium oxide shell to encapsulate EGaIn, just as aluminum oxide encapsulates aluminum. This sounds like a good thing, but it makes it much more difficult to make composites with EGaIn because it becomes non-conductive, and we use EGaIn for its high electrical conductivity in many cases. The solution is also very simple, just break the oxide shell, and when the EGaIn inside flows out (because it is a liquid metal), it will form a conductive path through the percolation. The most straightforward way to activate is to choose a stiffer elastomer because they are less likely to deform during activation (e.g., mechanical force applied by pressing)

and cause activation failure. Behind the successful activation is the choice of stiffer elastomers that bring lower stretchability as stretchable electrons which is not a good sign.

Therefore, the use of softer elastomers for LMEC is often proposed by researchers, but the idea is easy to come up with, the method takes time. However, we have a promising hypothesis to address this challenge to achieve high tensile conductivity composites with soft elastomers and EGaIn.

3. Motivations

I will present three questions encountered in this study, and hypotheses for solutions.

3.1. Can conductive LMEC be successfully synthesized from highly stretchable silicone elastomers with particle sizes approaching 1 micron?

First, as mentioned in the previous section, at this stage, softer elastomers are difficult to use for LMEC because it is difficult to break the oxide shell of EGaIn by deformation when mechanical stress is applied. Moreover, the size of the EGaIn particles is also an important indicator for the production of LMEC. The smaller the particle size, the better, because larger particle sizes (20-100 microns) may cause damage or leakage during the use of the LMEC, which greatly reduces the value of the LMEC application. Moreover, small particle size is more suitable for printing and is the key to making printable circuits. However, the small size (1-5 microns) poses a difficult problem in that it requires greater mechanical force to activate, as described in Chapter 1.2, making it difficult to form a conductive path.

Therefore, we propose a surface modification method to encapsulate the surface of EGaIn with polyvinylpyrrolidone (PVP). PVP has bonding-enhancing properties and its good phase properties with EGaIn allow it to be used as a dispersant for EGaIn.[13,38] In LMEC, PVP may play a very important role because surface modification has a high potential to weaken the interface between EGaIn and elastomers. If the surface modification is successful, it is very likely that we can use smaller EGaIn particle size combined with high stretching soft elastomeric system to make LMEC with super high electrical conductivity and stretchability, which perfectly meets the requirements of stretchable electronic applications.

3.2. Do the LM microparticles increase in size upon dispersion in an elastomer?

After microscopic image comparison, we found that the particle size of EGaIn particles seems to increase after the shear mixing process. This step is to disperse the elastomer with EGaIn particles

to form a composite. In order to confirm the increase of particle size, we will measure several different material combinations, both before and after shear mixing.

Also, we will try to use different particle size measurement methods to find the particle size of EGaIn particles to get more accurate comparison results. ◦

3.3. Does the electromechanical response of LM-based conductors depend on the rate of applied deformation?

The choice of displacement rate is an issue for any researcher performing tensile testing, but we have not found systematic studies. Generally, a low, very low shift rate is chosen for testing stretchable electronics to avoid damage to the sample during high speed stretching. However, we found after a brief test that high displacement rates may have higher electromechanical stability if the sample is allowed.

Therefore, we made a hypothesis that different shift rates may have different electromechanical responses. A series of tests were conducted with LMEC as the test subject. Of course, since there is no previous research to support this, we need a comparator. We will introduce an LM-based conductor to conduct the same experiment for comparison to verify the accuracy and replicability of the experiment.

4. Experiments

4.1. Liquid Metal Elastomer Composite Formulation

The liquid metal elastomer composite (LMEC) was prepared by mixing eutectic gallium indium (EGaIn) with polyvinylpyrrolidone (PVP; Thermo Scientific Chemicals) and Ecoflex 00-30 (Smooth-On). Eutectic gallium-indium was prepared by prior mixing 75 wt.% gallium and 25 wt.% indium. A 20 ml glass vial is prepared, and the entire manufacturing process will take place in the glass vial. The appropriate amount of PVP (2-10 wt.% relative to EGaIn) was added to the vial and the ratio of PVP with different molecular weights was determined (normally, MW: 10,000 and 1,300,000 = 1:1). Add 10 ml of isopropyl alcohol (IPA; Fisher Scientific) and dissolve PVP at room temperature for approximately three to twelve hours depending on the amount of PVP, which can be accelerated by bath-sonication (Cole-parmer, 8890). Slowly add 2.5 g of EGaIn droplets to the vial with a syringe. The vial was placed on the vortex mixer (Thermo Scientific, LP Vortex Mixer) for two minutes and 2000 rpm to reduce the size of the EGaIn droplets by oscillation to make the subsequent sonication process more efficient. Using the probe sonicator (Branson, Sonifier SFX 550) to reduce the size of EGaIn particles, different particle sizes were obtained by adjusting the power and duration, usually 15% power and 2 min 30 sec were used in this study. EGaIn particles were sedimented by placing the vial at room temperature for 24 hours, after which the IPA was decanted. Add Ecoflex 00-30 parts A and B to the vial separately, usually using a 1A:1B ratio. The Ecoflex and EGaIn were thoroughly dispersed by a planetary shear mixer (FlackTek SpeedMixer, DAC 150.1 FVZ-K) for two minutes at 2500 rpm. In summary, in volume fractions, the composition of EGaIn and Ecoflex 00-30 was 65% and 35%.

4.2. Tensile Specimens Formation

Ecoflex 00-30 (Smooth-On) parts A and B were added to a plastic cup at a 1A:1B mass ratio and mixed by a planetary shear mixer (FlackTek SpeedMixer, DAC 150.1 FVZ-K) for 1 min and 2500 rpm. Pour Ecoflex 00-30 into the acrylic mold with the size of 70 × 10 × 0.15 mm^3. Place the plastic cups at room temperature for 6 hours to cure Ecoflex 00-30 substrate. Apply silver tapes (GENNEL, 5 mm width) to both sides of the substrate. Print the ink on the substrate, making sure the ink has overlap to the silver tapes. Wait at room temperature for 24 hours, then place the print specimen in the oven for 30 minutes at 60 °C. Either prepare a mold of the same size to be mounted on top of the specimen or simply pour the remixed Ecoflex 00-30 (1A:1B) onto the print circuit,

making sure it covers the pathway and the area where it overlaps with the silver tapes. Cured at room temperature for 6 hours and ready for use.

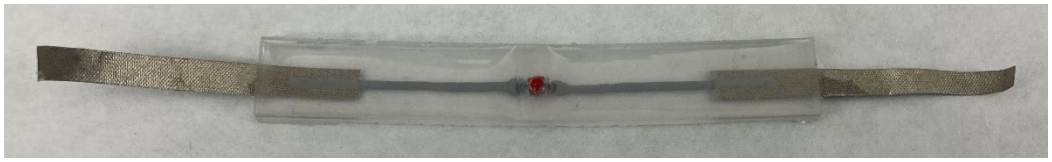

Figure 6 Tensile specimen with mounted LED

4.3. Printing Process

A high-precision dispenser system (Musashi Engineering, ML 808GX) equipped with a 3-axis robotic arm was used for direct-writing LMEC. Transfer the LMEC to the syringe and print with a 32-gauge needle at 50 kPa and 8 mm s^{-1}. The tensile specimens in this study were all 50mm long.

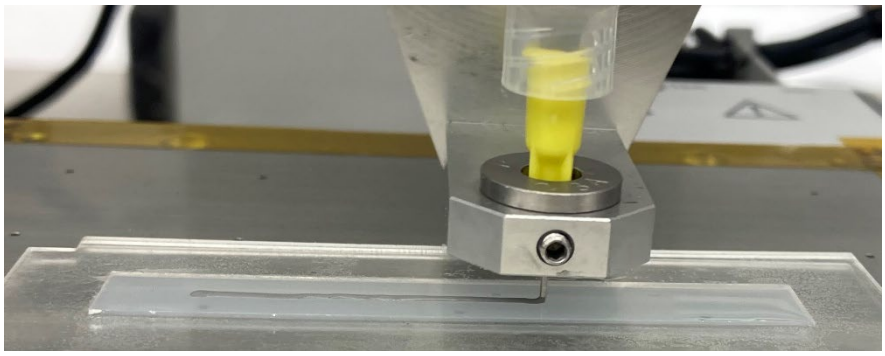

Figure 7 Printing illustration of LM composites

4.4. Electromechanical Characterization

The tensile specimens were stretched under controlled conditions. The tensile specimens were strained by a linear actuator. A voltage divider and an external power supply (Electro Industries, DIGI 35A) were used to measure the electrical resistance response of conductive pathways. LabVIEW and Arduino were used to collect the data of electrical resistance and control the linear actuator, respectively.

4.5. Microscopy Imaging

The micrograph was obtained with an optical microscope (Leica DMi1). Scanning electron microscopy (SEM) was conducted on an FEI Sirion XL30 operating at 5 kV for the samples.

5. Results and Discussions

5.1. EGaIn synthesis

In this chapter, the synthesis of liquid metal complexes from scratch and the analysis of their properties under different conditions, including particle size, electrical conductivity (resistance), etc. are mentioned in a step-by-step manner. The order of the chapters is the same as the progress of the study.

The effects of PVP coating with two different molecular weights, 10,000 and 1,300,000 g/mol, on the characteristics of EGaIn particles were revealed by Jo et al.[13] The two molecular weights displayed different binding mechanisms with the elastomer, according to the authors' observations. In particular, it was discovered that low molecular weight PVP binds to the elastomer close by, whereas high molecular weight PVP, which has higher steric hindrance, can bind to the elastomer farther away. The interaction between EGaIn particles and elastomer was found to be improved by using two different molecular weights of PVP, which increases the shear stress between them during stretching. This indirectly weakened the solid-liquid interface of the EGaIn particles and allowed the strain-activation phenomenon to take place.

5.1.1. Development and Challenges of LMEC for Soft Elastomers

The development of strain-activated ink posed a significant challenge yet an essential step in the experimental process. This thesis aims to provide an extensive account of the production process and the challenges encountered during the development of the ink. The conductive ink used in this study is based on the recipe and production process described by Jo et al.,[13] with modifications made to accommodate the use of soft elastomers. The adjustments mainly involve material ratios and production processes, with a particular focus on the addition of PVP and particle size. The addition of PVP significantly affects the strain-activation process, which will be further discussed in the subsequent section. On the other hand, particle size plays a crucial role in printability and activation, with excessively large particles impeding printability and excessively small particles hindering oxide shell rupture during strain, thereby preventing activation and conductive pathway formation.[13,46]

5.1.2. Control the Particle Size Using Sonication

To achieve the desired particle size of approximately 1 μm, we employed the probe sonication technique, which is found to be more efficient than overhead mixing. However, this technique poses challenges in controlling particle size distribution. In our study, we aimed to achieve a

balance between LMEC activation and printability by adding PVP at 2 wt.% relative to EGaIn and adjusting the EGaIn-to-Ecoflex volume fraction while keeping the ultrasound coefficient constant at 10% power and a duration of two minutes. Samples of EGaIn and Ecoflex with different volume fractions were tested for their activation capability. Ecoflex with volume fractions of 26%, 38%, 45%, and 58% were coated onto acrylic plates, which was activated by pressing to form conductive pathways. A sample is considered activated when a resistance is detected, and not activated when no resistance is detected.

Of the four different Ecoflex volume fractions samples, only the 58% sample fails to activate. The other three samples all show resistance, with the 26% sample having the lowest resistance. From these results, we can derive two conclusions: first, that 45% volume fractions of Ecoflex is the upper limit or maximum value for activation, and second, that reducing the volume fractions of Ecoflex and increasing the volume fractions of EGaIn can enhance the conductivity of the conductive path. Additionally, we observed that this ultrasonic coefficient (10% power and two minutes) caused uneven particle size distribution, possibly due to insufficient power and duration.

5.1.3. Volume Fraction of EGain-to-Ecoflex, 60% and 40%

In order to improve the uniformity of particle size, it appears essential to increase the power and duration of the sonication. Additionally, determining the volume fraction of EGaIn and Ecoflex are equally important. Initially, we attempted to modulate the volume fraction of EGaIn and Ecoflex to 60% and 40%, respectively, based on our previous experiment, which indicates that a volume fraction of Ecoflex below 45% is more likely to form a conductive pathway. Moreover, when the volume fraction of Ecoflex remains at a higher proportion, its stretchability properties would significantly improve, making it easier to produce high-stretchable electronics.

To reduce the complexity of the description, we abbreviate the power and duration of the ultrasonic coefficients as P&D, and the minutes and seconds as min and s. We attempted different P&D, including 10% for 3 min, 13% for 2 min 15 s, 15% for 2 min, and 15% for 2 min 30 s, and samples produced under these conditions can be activated, and the particle size is relatively concentrated. However, their low electrical conductivity makes these samples of little practical value and improving their conductivity has become the most pressing issue to be addressed. We attempted to increase the power of the sonication since higher power is more likely to produce a high

concentrated particle size distribution, indirectly increasing the number of EGaIn particles activated during the process to generate a better conductive pathway.

By increasing P&D to 17% and 20% for 2 min, we successfully obtained more uniform particle sizes, particularly for the sample with 20% power. However, as previously mentioned, small particle sizes (in the nanometer range) make it difficult to break the oxide shell and activate the conductive pathway successfully. Although we did obtain a high concentrated particle size distribution for the sample with 20% power, we were unable to measure its conductivity, indicating that the activation is unsuccessful. On the other hand, the sample with 17% power is successfully activated to form a conductive pathway. After increasing the power of the sonication, we did indeed obtain better conductivity, but it cannot be considered outstanding. We also found that particle size would affect the stretchability performance to some extent, with the stretchability decreasing when the particle size decreases to below one micrometer. Therefore, maintaining particle sizes within the range of one micrometer may produce the best samples.[13,46]

5.1.4. Volume fraction of EGain-to-Ecoflex, 65% and 35%

One of the most straightforward ways to improve electrical conductivity is to increase the volume fraction of EGaIn. However, if the volume fraction of Ecoflex is too low, its stretchability may be compromised. Therefore, the volume fraction of EGaIn was increased to 65% to obtain better conductivity while maintaining stretchability. We tried various P&D, including 13% for 2 min 30 s, 15% for 2 min, 15% for 2 min 30 s, 16% for 2 min 15 s, 17% for 2 min, 20% for 1 min 30 s, and 20% for 2 min. Under all these conditions, we were able to activate the samples. However, the samples produce under 17% and 20% power had tiny particles, resulting in reduced stretchability. Moreover, because the volume fraction of EGaIn is increased, there are more EGaIn particles, making activation easier and eliminating the need for highly concentrated particle size distribution.

Different P&D were measured the particle size of EGaIn through Optical Microscope (OM) images and manual image analysis (see chapter 5.2.2 for details). Specifically, the P&D of 13% for 2 min 30 s, 15% for 2 min 30 s, 16% for 2 min 15 s, and 17% for 2 min were used, resulting in average particle sizes of 1.63, 1.48, 0.8, and 0.89 μm, respectively, shown in Figure 6 - 9. Among them, Figure 6 shows the distribution plot of the P&D of 13% for 2 min 30 s, demonstrating a significant bimodal distribution with peaks at 0.6 and 1.5 μm, indicating a lack of particle size uniformity. Although the P&D of 16% for 2 min 15 s (Figure 8) and 17% for 2 min (Figure 9)

does not show significant bimodal distribution, their average particle sizes are close to nanoparticles, which is unfavorable for the formation of conductive pathways.[13,46] Therefore, 15% for 2 min 30 s (Figure 7) were selected as the optimal P&D for producing samples, with an average particle size of 1.48 μm and a uniform size distribution, resulting in lower resistance values after activation. With EGaIn particles of this size, we are able to achieve high stretchability without compromising activation potential, allowing us to obtain the desired properties without making any trade-offs.

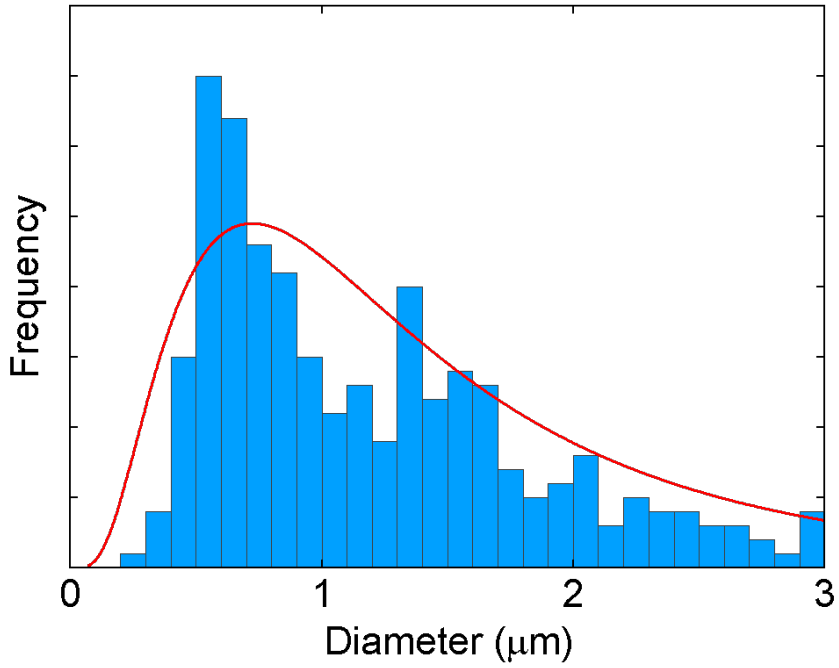

Figure 8 Size distribution of EGaIn particles with P&D 13% for 2 min 30 s

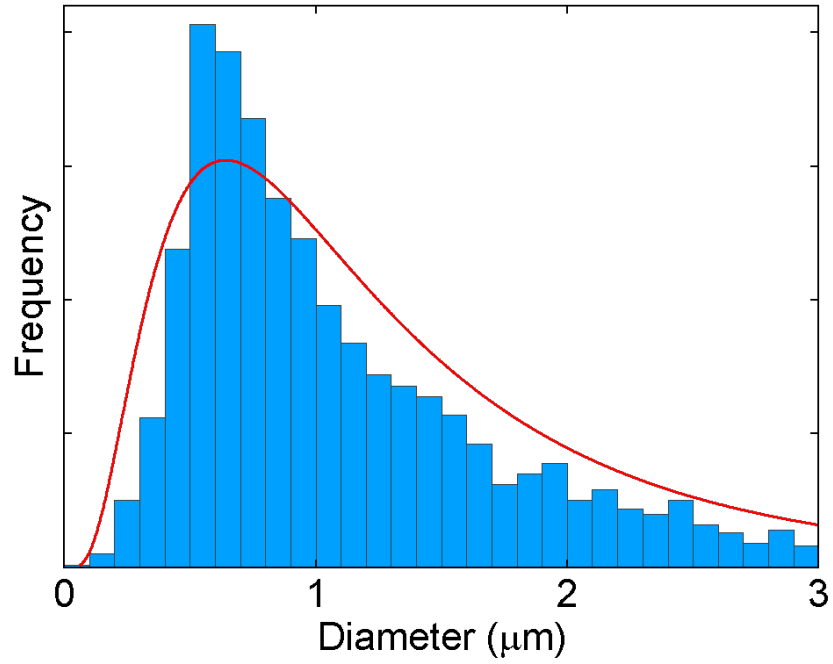

Figure 9 Size distribution of EGaIn particles with P&D 15% for 2 min 30 s

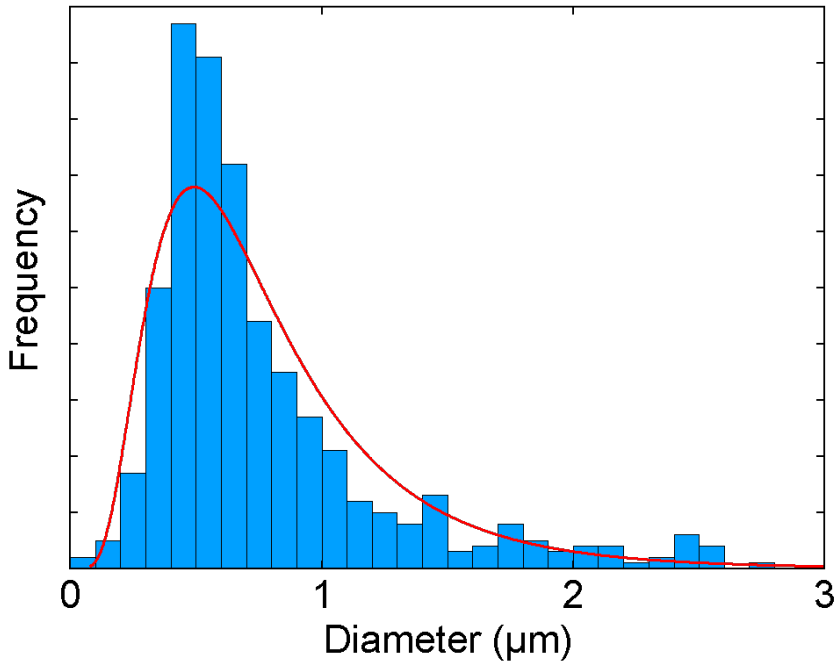

Figure 10 Size distribution of EGaIn particles with P&D 16% for 2 min 15 s

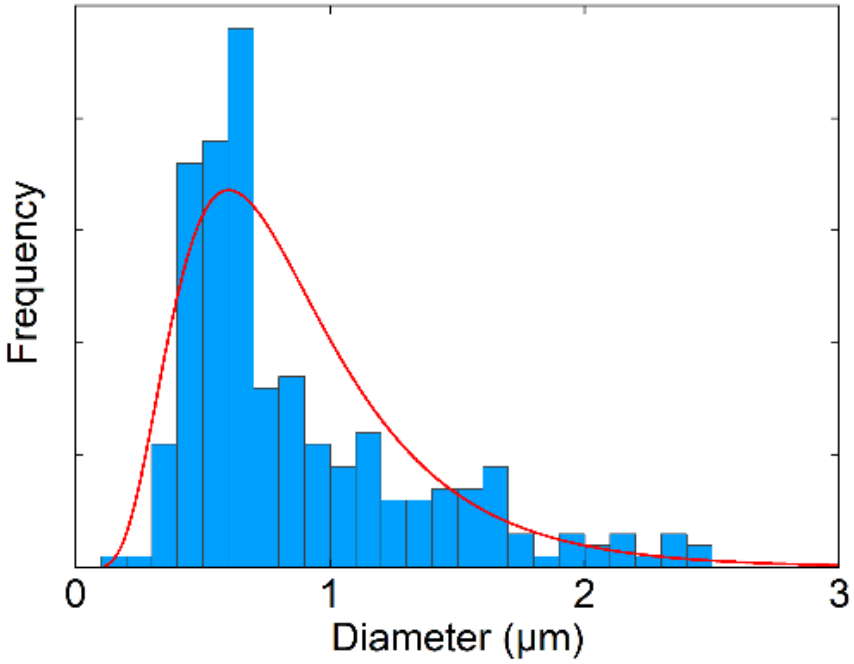

Figure 11 Size distribution of EGaIn particles with P&D 17% for 2 min

5.1.5. Architecture of Tensile Specimens

In previous experiments, ink was coated onto acrylic plates to enable rapid testing of samples under different conditions. However, the objective is to produce printable ink. Therefore, a high-precision dispenser system was incorporated into the process using a three-axis robotic arm for direct ink writing. Pure Ecoflex was synthesized as a printing substrate, and a 5 cm long straight pathway of LMEC was printed on it.

5.1.6. Strain-activation

The printing test was highly successful, and the resulting samples could activate conductive pathways through pressing or stretching, thereby facilitating the production of a strain-activated LMEC. Upon testing the resistance, it was found that the resistance value was approximately 1.4 Ω/cm. To emphasize strain-activation as the primary means of activation, the sample structure was modified after printing. The ink-printed samples were coated with an additional layer of synthesized pure Ecoflex to completely envelop the conductive pathways. This design was expected to improve conductivity, as the conductive pathways would experience greater shear stress from the surrounding Ecoflex during stretching, causing more oxide shells of EGaIn

particles to rupture. Experimental results confirm the hypothesis. This new sandwich-structured sample measured 1 Ω/cm, indicating that this structure can better activate the conductive pathways.

5.1.7. Volume Fraction of EGain-to-Ecoflex, 75% and 25%

Driven by curiosity about whether the volume fraction of EGaIn could be further increased, we tested a volume fraction of 75% EGaIn. The measured resistance was astonishingly high, as the sample only achieved approximately 1.8 Ω/cm under the same printing conditions and structure. Compared to the 65% volume fraction, the conductivity of the 75% volume fraction was only half of the former. The cause of this result was likely due to the incompleteness of strain-activation. As mentioned earlier, during strain-activation, the elastic body applied shear stress to the EGaIn particles, causing the oxide shells to rupture and form a conductive pathway. However, when we added too high a proportion of EGaIn, the relative reduction in the number of elastomers capable of applying shear stress led to a reduction in the number of particles receiving shear stress, resulting in a strange phenomenon where the increase in EGaIn particles led to a deterioration of the activation. This result demonstrates that simply increasing the proportion of liquid metal cannot necessarily improve the conductivity value; the compatibility between materials is also important.

5.1.8. Investigation of Conductive Properties of LMEC

The successful synthesis of LMEC was only the beginning of the experimental process, as there were still many properties that needed analysis. Since the particle size and addition ratio of EGaIn had been confirmed previously, our attention was turned to PVP and Ecoflex. By altering the synthesis ratios, we observed changes in conductivity and searched for a more optimal formula.

5.1.9. Saturation Curve of PVP

Once the volume ratio and particle size of the liquid metal and elastomer were determined, we turned our attention to examining the potential effect of PVP addition on the resulting electrical conductivity performance. Thus, we also conducted an analysis on the impact of saturation of PVP, a crucial material, on conductivity. Unlike previous research endeavors that employed relatively small amounts of PVP, we explored the effects of varied PVP quantities. While using probe sonication technique to reduce particle size, the addition of PVP did not significantly affect particle size, enabling the safe addition of more PVP and subsequent observation of outcomes. As shown in Figure 10, we investigated the weight percent of PVP with respect to EGaIn, ranging from 0 to 10 and equally employed both molecular weights of 10,000 and 1,300,000. As previously mentioned, the utilization of solely soft elastomers and EGaIn did not yield sufficient shear to

rupture the oxide shell. Consequently, the absence of PVP content (0 wt.%) in this printing pathway leads to a lack of electrical conductivity. However, subsequent to the addition of 2 to 6 wt.% of PVP, average resistance continues to decrease dramatically from 1.04, 0.91, to 0.19 Ω/cm, suggesting that PVP has yet to attain saturation. After that, the average resistance is 0.17 and 0.15 Ω/cm for 8 and 10 wt.% PVP, respectively. Obviously, after the addition of 6 wt.%, there is no significant change in the measured average resistance value, indicating that the amount of PVP has reached saturation. Moreover, the high quantity of PVP added increases the interconnection with the elastomer matrix, thereby facilitating strain-activation.

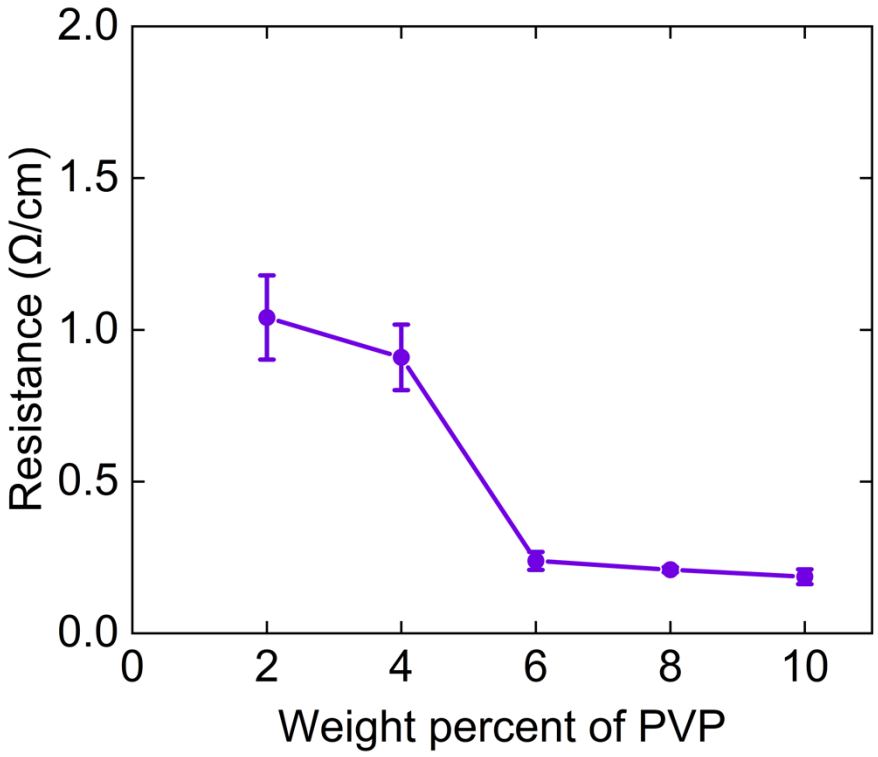

Figure 12 Electrical resistance of the activated samples as a function of PVP weight percent difference

5.1.10. Different Molecular Weight Ratios of PVP

Jo et al.[13] revealed the impact of PVP coating with two different molecular weights (MW), 10,000 and 1,300,000 g/mol, on the properties of EGaIn particles. The authors observed that the two molecular weights exhibited distinct binding mechanisms with the elastomer. Specifically, low-molecular-weight PVP was found to bind to the elastomer in the surrounding areas, while high-molecular-weight PVP, which had higher steric hindrance, was able to bind to the elastomer further away. The use of two molecular weights of PVP in combination was found to enhance the interaction between EGaIn particles and elastomer, thereby indirectly weakening the solid-liquid

interface of EGaIn particles and enabling the strain-activation phenomenon to occur. We investigated the effect of weight ratios of two molecular weight additions on the electrical conductivity. Without changing the total weight of PVP (6 wt.%), we varied the weight ratios of the two molecular weights, 10,000 and 1,300,000 g/mol, as 9:1, 7:3, 5:5, 3:7, and 1:9.

As shown in Figure 11, surprising results were obtained, showing a saturation curve. When the ratio of PVP with a molecular weight of 10,000 to 1,300,000 is 9:1, the average resistance value is approximately 1.5 Ω/cm, which is not considered favorable. However, when the ratio is reduced to 7:3, the average resistance value decreases significantly to an excellent value of 0.38 Ω/cm. By further reducing the amount of PVP with a molecular weight of 10,000, an average resistance value of 0.24 Ω/cm, which was previously obtained for 6 wt.% PVP, is achieved. Interestingly, as the amount of PVP with a molecular weight of 10,000 was decreased and the amount of PVP with a molecular weight of 1,300,000 was increased, the average resistance value does not decrease any further and reached saturation. The average resistance values of 3:7 and 1:9 in Figure 11 are similar to that of 5:5, with values of 0.23 and 0.18 Ω/cm, respectively. There are various possible explanations for this phenomenon, the two most likely being: firstly, although Jo et al.[13] revealed the different roles played by PVP with different molecular weights, with longer and shorter chains of molecules being able to pull both nearby and distant elastic bodies, making it easier to break the oxide shell of EGaIn when activated. However, the aforementioned study was based on rigid elastomers and not the soft elastomers used in this research. It is possible that soft elastic bodies require more longer chain PVP to stabilize distant elastic bodies and improve the efficiency of breaking the oxide shell. Secondly, adding more PVP with a molecular weight of 1,300,000 significantly increases the viscosity, which reduces the efficiency of the sample during sonication and causes a slight increase in particle size. This is also why, even though the amount of PVP with a molecular weight of 1,300,000 was increased significantly, the average resistance value decreases only slightly, because the increase in particle size is small. Nonetheless, larger EGaIn particles can still achieve a smaller resistance value due to better breakage of the oxide shell. In any case, the 5:5 ratio of molecular weights used in this study still holds value and can continue to be used.

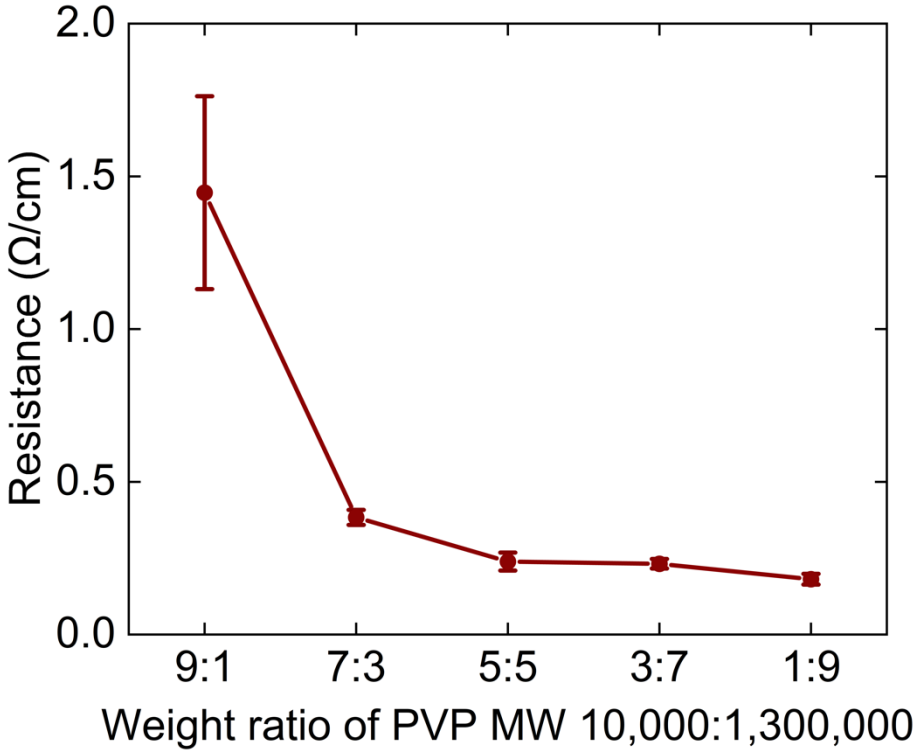

Figure 13 Electrical resistance of the activated samples as a function of PVP molecular weight ratios, 10,000 and 1,300,000

5.1.11. Different Weight Percentages of PVP With a Molecular Weight of 1,300,000

In the previous chapter, we observed that high-molecular-weight PVP had a greater impact on activating the conductive pathway compared to low-molecular-weight PVP. Thus, we designed another set of experiments with a PVP molecular weight of 1,300,000 (1.3M PVP). We selected 1.3M PVP weight percentages ranging from one to four as variables and measured their resistances of the conductive pathway. The resistance results are shown in Figure 12. Consistent with our previous inference, using only 1.3M PVP is sufficient to achieve comparable or even better conductivity properties compared to using a mixture of both molecular weights. To facilitate comparison, we present Figure 10 - 12 in Figure 13, from left to right.

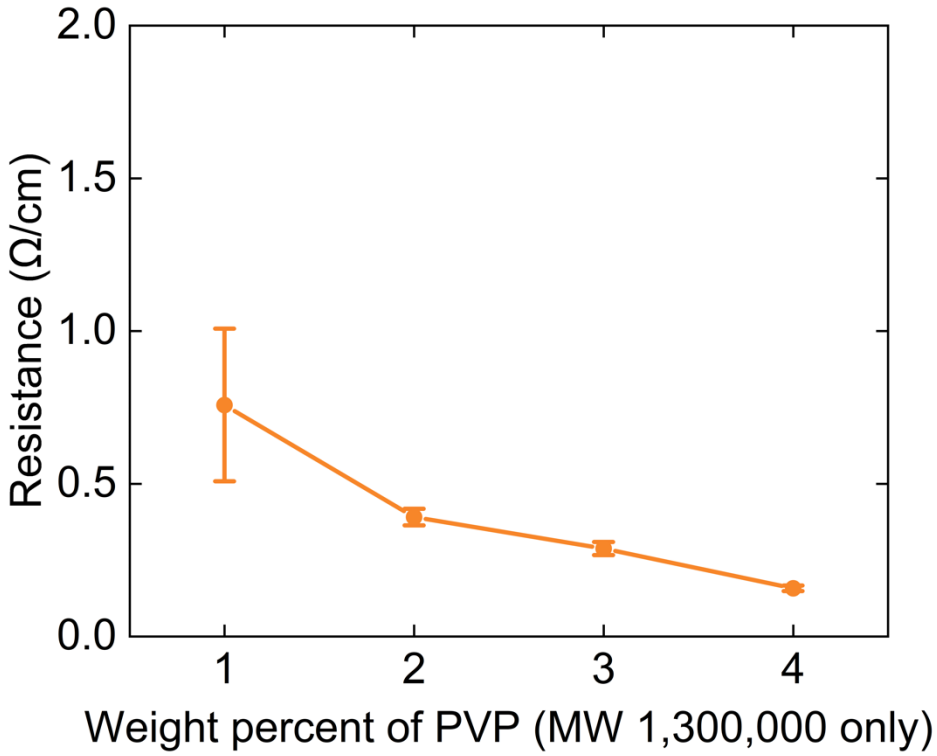

Figure 14 Electrical resistance of the activated samples as a function of weight percentages of PVP with a molecular weight of 1,300,000

In Figure 13, the average resistances for the 1 wt.% sample on the right plot and the 2 wt.% sample on the left plot with the same amount of 1.3M PVP are 0.76 and 1.04 Ω/cm, respectively, indicating a significant difference in resistance. Before comparing the sample with 7:3 molecular weight ratio in the middle graph, let's do a simple calculation, its 1.3M PVP is 6wt.%*0.3=1.8wt.%, which is approximately equal to 2wt.%, so we can analyze it together with the other two graphs. The conductivity of the same 2 wt% of 1.3M PVP with low-molecular-weight (MW 10,000) PVP of 2, 4 and 0 wt.% of the three samples shown from left to right in Figure 13 has an average resistance of 0.91, 0.38 and 0.39 Ω/cm, respectively. It can be observed that the average resistance of the latter two samples is almost the same, indicating that high electrical conductivity can be achieved by using either a high content of high-molecular-weight PVP alone or a large amount of low-molecular-weight PVP. When the concentration of 3 wt.% of PVP with a 1.3M PVP is compared to the 6 wt.% concentration in the left plot (same as the sample in the middle plot, not compared), the average resistances were 0.28 and 0.19 Ω/cm, respectively. The result shows that using only 1.3M PVP does not yield the best conductivity. However, a reversal appears when the concentration was changed to 4 wt.%, which is equivalent to the 4.2 wt.% concentration in the

middle plot (6 wt.% * 0.7 = 4.2 wt.% ≈ 4 wt.%). The average resistances of the three samples in Figure 13 from left to right are 0.17, 0.23, and 0.15 Ω/cm, respectively, all exhibiting excellent conductivity. These experimental results indicate that using only high-molecular-weight PVP can also yield excellent conductive pathways, providing us with another option.

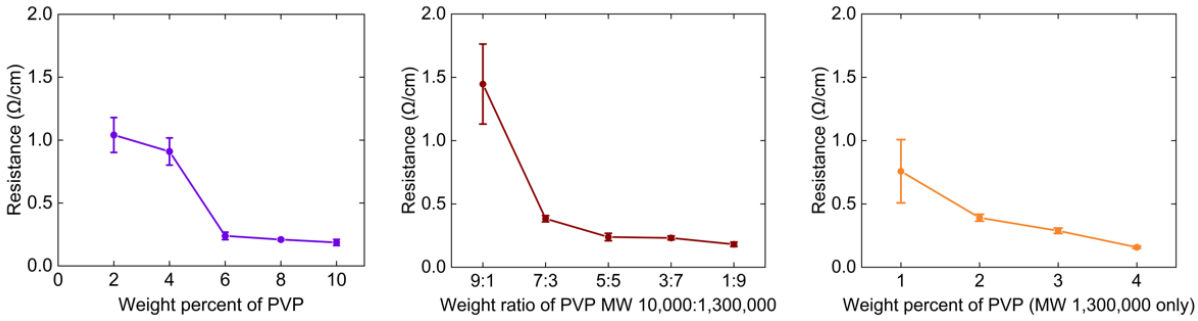

Figure 15 The electrical resistance comparison, from left to right, is shown in Figure 10-12

5.1.12. Different Ratios of Ecoflex Synthetic Units A & B

After investigating the effects of PVP addition and ratio on conductivity, our focus returned to Ecoflex. Previously, we discussed the volume fraction of EGaIn in Ecoflex and confirmed that a ratio of 65:35 exhibits the most comprehensive performance. Ecoflex is composed of synthetic units A and B, and the vast majority of users synthesize it in a 1:1 ratio. We conducted a separate experiment to study the effect of the ratio of Ecoflex part A and B on the LMEC. Under the premise of selecting the optimal ratio and not changing the amount of Ecoflex, we adjusted the ratio of synthetic units A and B in Ecoflex to 9:1, 7:3, 3:7, and 1:9, respectively. As shown in Figure 14, after measuring the resistance of samples with different ratios, the results were not significantly different. The average resistance of all samples is distributed around 0.23 Ω/cm and changing the ratio of synthetic units in Ecoflex does not cause any incidents of incomplete or failed activation. The reason for this may be attributed to the free monomer units of Ecoflex, namely that it does not completely react. If we attempt to overlay a layer of Ecoflex on already cured Ecoflex (both 1A:1B), there will be no obvious seam between the old and new layers. Therefore, we can infer that only a small number of precursors are required to participate in the curing process. To prove this inference, we can see in Figure 14 that the 9:1 and 1:9 ratios resulted in significant differences in the composition of synthetic units, but it does not affect the activation of the conductive pathway, indicating that fewer precursors are used for curing than expected. Further explanation of the electromechanical nature of 9:1 and 1:9 will also be given in Chapter 5.3.3.

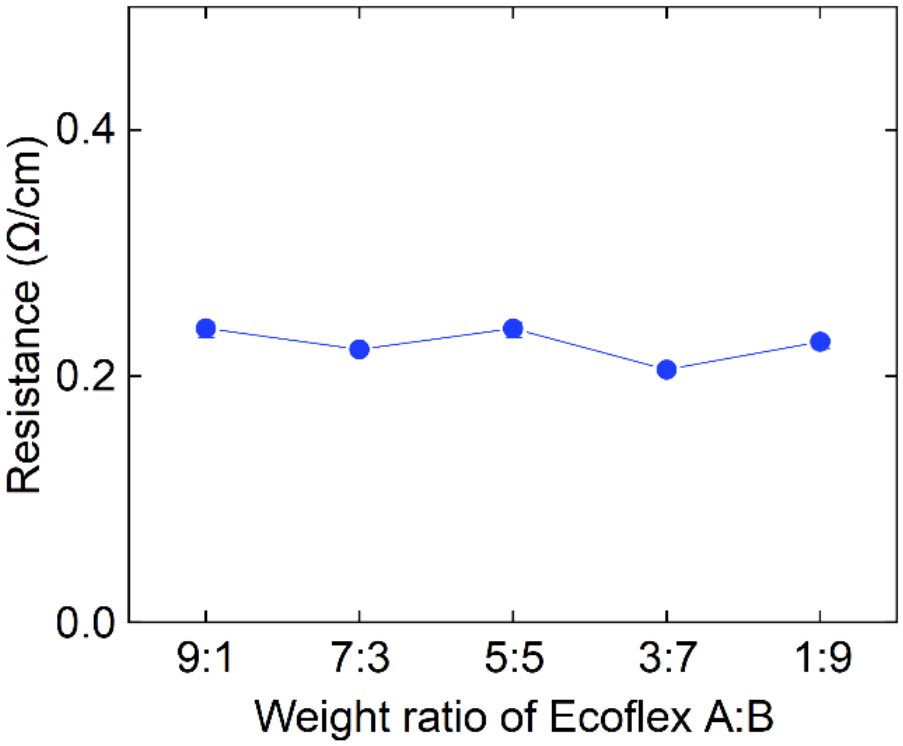

Figure 16 Electrical resistance of the activated samples as a function of different ratios, Ecoflex part A and B

5.2. Exploration of Particle size

In the previous chapter, we discussed the influence of sonication on particle size. In this chapter, we will elaborate on the measurement of particle size and the effects of the production process on particle size.

5.2.1. Particle Size Analysis: Image Analysis vs. Dynamic Light Scattering

In the scientific community, various methods exist for determining particle size. This study aimed to utilize two methods, image analysis and Dynamic Light Scattering (DLS), to evaluate and discuss the most appropriate technique for analyzing the LMEC.

5.2.2. Image Analysis for Particle Size Measurement

This method of measuring particle size could be simple yet effective by performing automatic or manual image analysis on well-captured optical microscopy (OM), scanning electron microscopy (SEM), or transmission electron microscopy (TEM) images to determine particle size. When a sufficient number of microscopy images are available, manual image analysis can be performed first, and the resulting data can be used for machine learning to facilitate subsequent automatic image analysis. Alternatively, automatic analysis can be carried out using the ImageJ software invented by the National Institutes of Health. In most cases, ImageJ can quickly detect particle contours and determine particle size or area. However, LMEC do not meet the prerequisite for rapid particle size measurement using ImageJ, i.e., clear particle contours. As shown in Figure 15, even if different particles can be easily distinguished by the human eye, ImageJ cannot recognize them. Therefore, manual image analysis is the only feasible option.

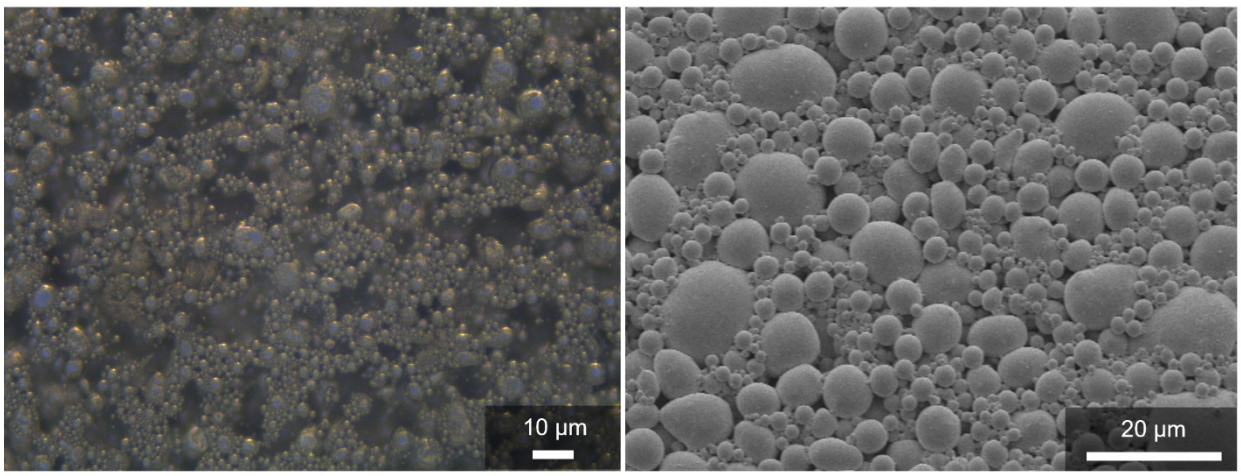

Figure 17 The micrograph and SEM Images of EGaIn particles, left to right order

Manual image analysis, as the name suggests, involves manually labeling each particle to obtain a size distribution chart. In practice, this method is not only time-consuming, but also depends on the quality of the microscopy images. When the image resolution is high and the picture is clear, the results of the particle size analysis are more accurate. Conversely, when the resolution is not high enough, the accuracy of the size distribution chart is affected due to difficulties in identifying the contours and boundaries of smaller particles and having no impact on larger particles. As shown in Figure 16, in this experiment, the particle size was manually marked using the micrographs and SEM images, and each sample under a single condition had more than 500 particle size marks to ensure sufficient accuracy.

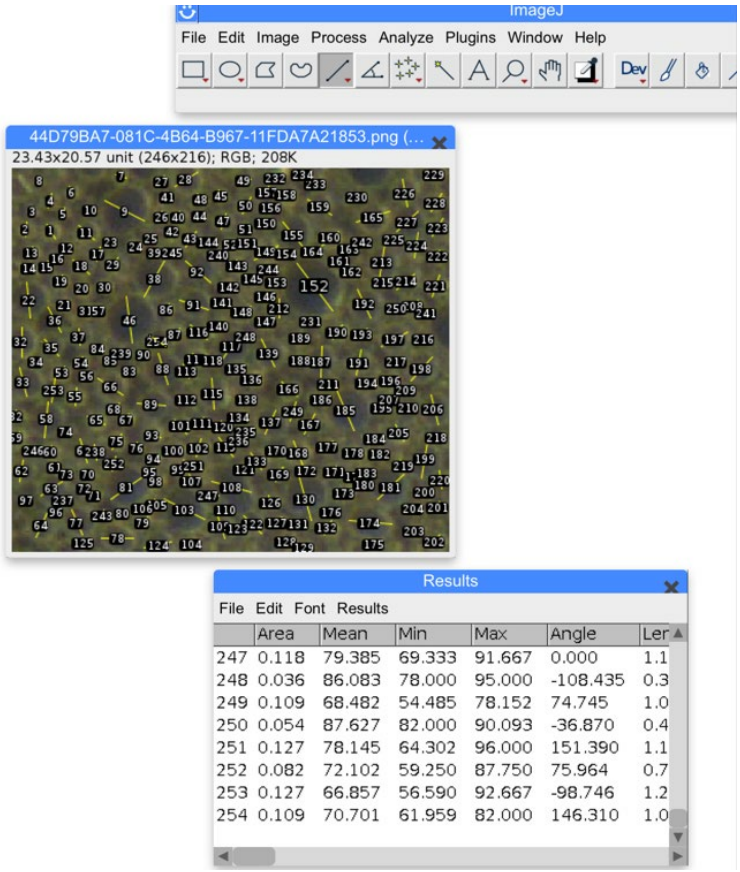

Figure 18 Method of manual image analysis by ImageJ

Using the above method, we measured the particle size of our prepared LMEC and obtained the distribution plot shown in Figure 17. This distribution plot contains over three thousand particle size data, and the width of each bin is 0.1 μm. The maximum and minimum particle sizes are 10.75 μm and 0.27 μm, respectively, with a median size of 1.25 μm and an average size of 1.61 μm. By

observing the particle size distribution plot, we can easily see that the peak of the size is concentrated around 1 µm, and the red distribution curve shows the highest value at 1 µm. Similar to the discussion in Chapter 5.1.2 on the relationship between ultrasonic power, time, and particle size, the particle size distribution is scattered, but there is no second peak. It should be noted that adding more polymers would affect the SEM imaging and result in a blurred image. Therefore, we could only use the micrographs for image analysis when measuring particle size, making it difficult to accurately measure particles close to the nanoscale. Therefore, we estimate that the particle size of this LMEC is slightly smaller than the measured value. However, as discussed in Chapter 5.1.4, the ideal average particle size for strain-activation is around 1 µm or slightly larger, so even if the particle size is slightly smaller, it still meets the requirement.

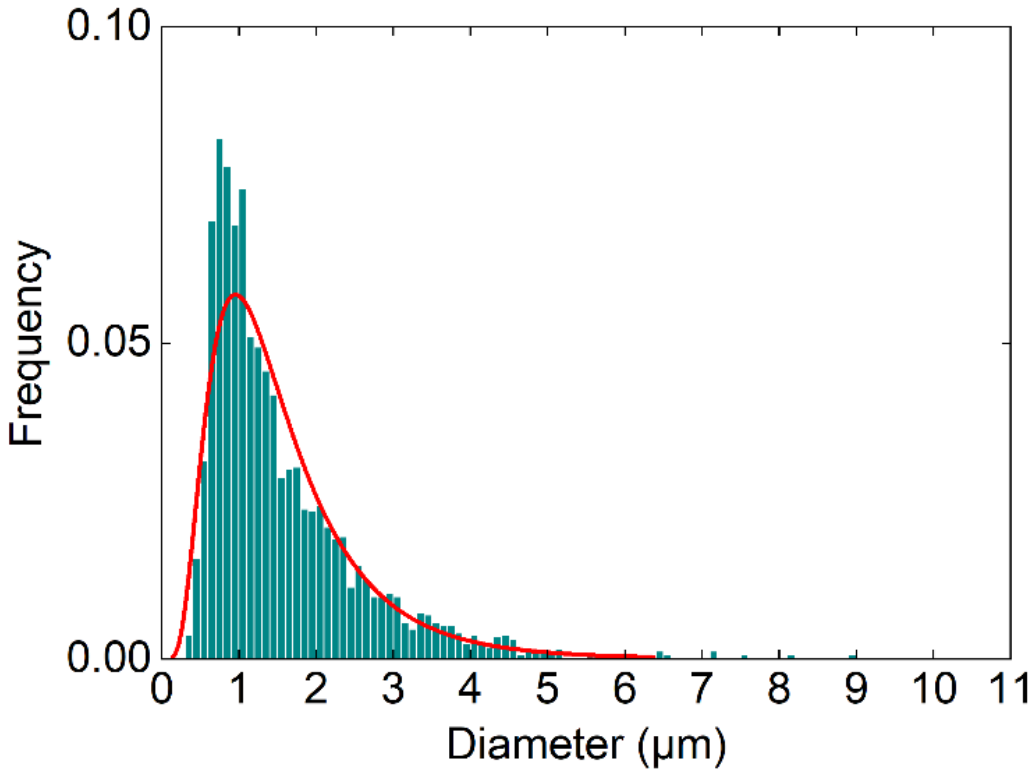

Figure 19 Size distribution of LMEC by manual image analysis

5.2.3. Dynamic Light Scattering for Particle Size Measurement

Dynamic Light Scattering (DLS), also known as Photon Correlation Spectroscopy, is a widely-used technique to measure the particle size distribution of suspensions. However, in the case of bulk EGaIn, DLS is not suitable for particle size measurement. Nonetheless, after reducing the

particle size to the micrometer range via sonication and diluting the sample, it is possible to measure the particle size using DLS. Due to the lack of precise information on the refractive index of EGaIn, we compare the results of image analysis with those obtained from experiments with different refractive indices. Through literature research, we found that the refractive indices of GaInAs and GaInAsP are 3.912 and 3.436, respectively, and we predicted that the refractive index of EGAIN falls within the range of 3.5 to 4. We conducted 15 particle size measurements with a 0.1 interval of refractive index, except for the sample with a refractive index of 3.5, which was measured three times, while the other samples were measured twice (30 times in total) using the pure EGaIn suspension diluted with IPA. As shown in Figure 18, the result of the sample with a refractive index of 3.5 shows a bimodal distribution in the blue curve, which can be simply explained by the occurrence of aggregation or precipitation of some EGaIn particles during the third measurement (PVP was not used in this experiment). By observing the other curves, it can be noted that the green curve is consistently lower than the red curve, indicating a less concentrated particle size distribution. This was also due to the measurement order, where the red curve represents the first measurement, and the green curve represents the second measurement, which caused aggregation or precipitation due to the longer waiting time.

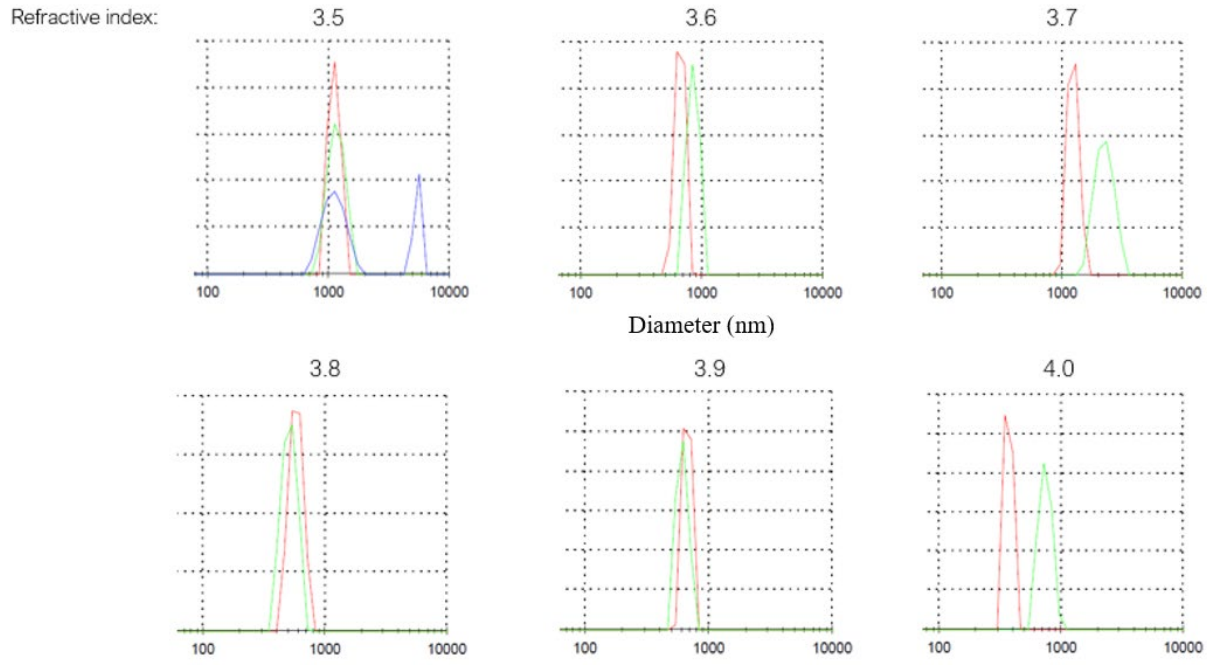

Figure 20 Size distribution of EGaIn particle with different refractive index by DLS

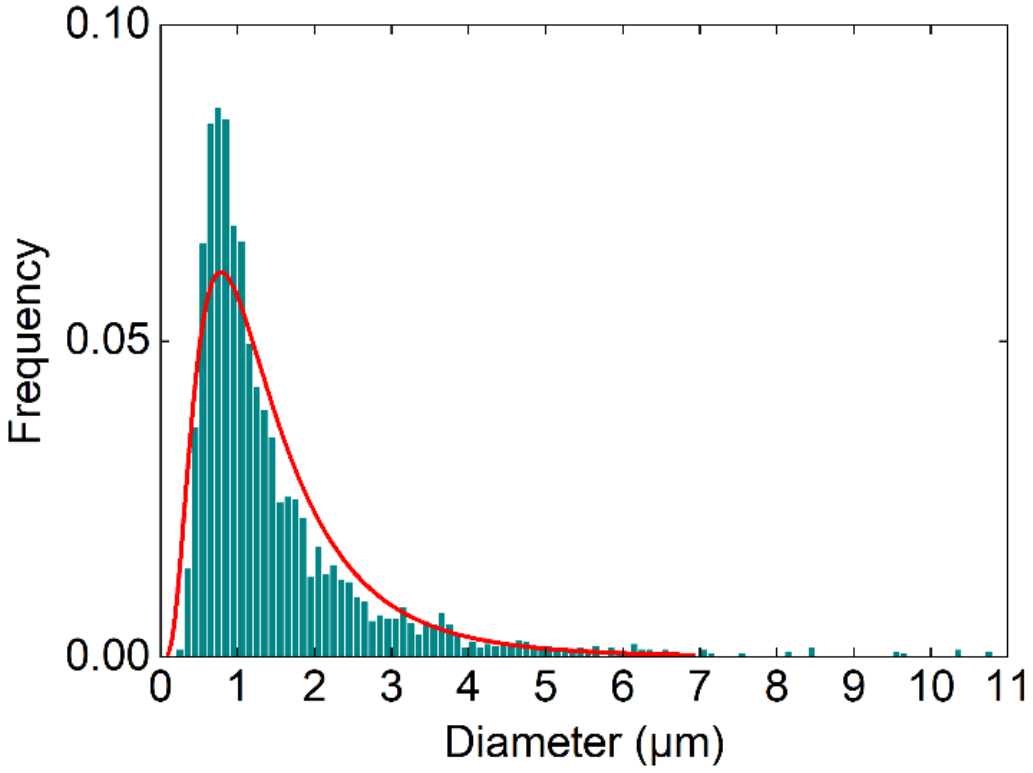

Figure 21 Size distribution of EGaIn particle by manual image analysis

In order to determine the most suitable refractive index for measuring the particle size of EGaIn using Dynamic Light Scattering (DLS), we compared the particle size data obtained through image analysis with those obtained using DLS. The peak of the particle size distribution in Figure 19 was found to be located at 0.8 μm, while the refractive indices of 3.5 and 3.6 in Figure 18 were found to be the closest to this value. Among them, the refractive index of 3.6 was found to be the closest to 0.8 μm. Therefore, we recommend using a refractive index of 3.6 for DLS particle size analysis. By comparing the two methods for measuring particle size, we found significant differences between them. DLS infers particle size through scattered light and requires the sample to be diluted to a point where light can pass through it. However, this prerequisite determines that DLS will not measure larger particles, resulting in differences from the real situation. Furthermore, removing the larger particles causes the overall average particle size and the peak value of the distribution curve to shift leftwards and become more concentrated. In conclusion, there are still many problems with using DLS to measure the particle size of EGaIn, and AI image analysis is expected to become a more promising tool for future measurements.

5.2.4. Shear Mixing and Its Effect on EGaIn Particle Size

According to my second study question, the effect of shear mixing on EGaIn particles appears to amplify their size. This observation was made during the fabrication of LMEC, where the micrograph (OM) images were recorded after each processing step. The final step involves shear mixing of the added Ecoflex and EGaIn. Upon examination of the micrographs before and after shear mixing, we were surprised to find that the particles appeared to have increased in size, as depicted in Figure 20. To confirm our suspicion, we measured the particle size before and after shear mixing.

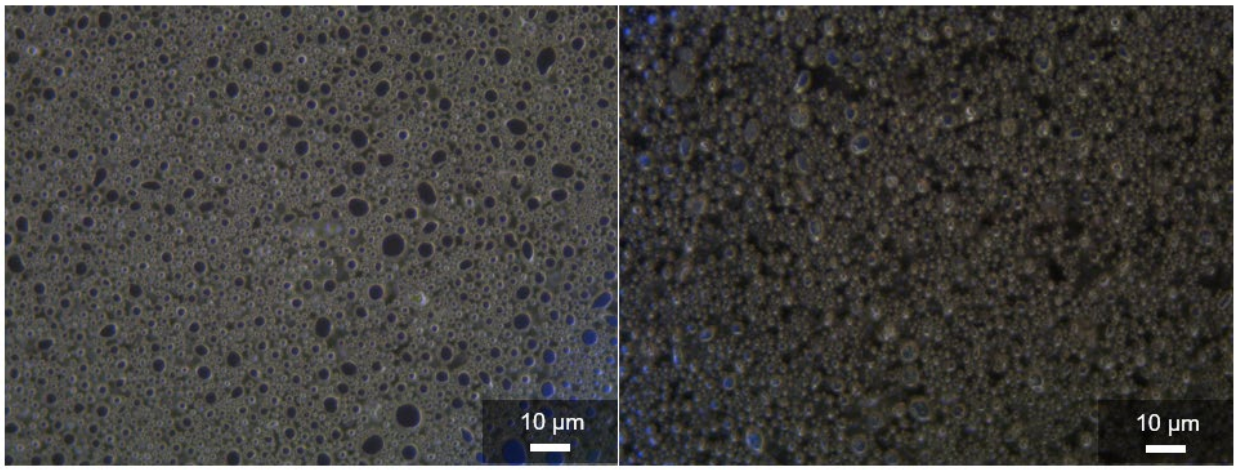

Figure 22 The micrograph images of LMEC before (left) and after (right) shear mixing

To comprehensively examine this hypothesis, we arranged the three materials used in the LMEC to obtain all possible results. A total of six cases were measured for particle size, including pure EGaIn (none)(S), EGaIn + PVP (none)(S), EGaIn + Ecoflex (S), and EGaIn + PVP + Ecoflex (S), where (S) indicates the presence of shear mixing and (none) indicates on shear mixing. The latter two cases only have the particle size after shear mixing, as both Ecoflex and EGaIn need to be uniformly mixed through shear mixing.

5.2.5. Particle Size Distribution Analysis – 1st

Figure 21 presents the comparison of particle size distributions before and after shear mixing for pure EGaIn and EGaIn + PVP. Observing the two distribution plots, we can see that the change in particle size before and after shear mixing is minimal. The most significant difference is that the peak of the distribution curve becomes higher, indicating that the particle size distribution is more concentrated after shear mixing. Specifically, comparing the pure EGaIn particle size data, the average particle size is 1.278 µm and 1.228 µm (S) before and after shear mixing, respectively.

Surprisingly, the average particle size decreased after shear mixing, and the median particle size is 1.04 μm and 0.975 μm (S), respectively. Furthermore, comparing the EGaIn + PVP particle size data, the average particle size is 1.17 μm and 1.237 μm (S) before and after shear mixing, respectively. The average particle size slightly increased, and the median particle size for both cases is 0.944 μm. In summary, we can conclude that shear mixing does not significantly increase the particle size of EGaIn in either pure EGaIn or EGaIn + PVP systems.

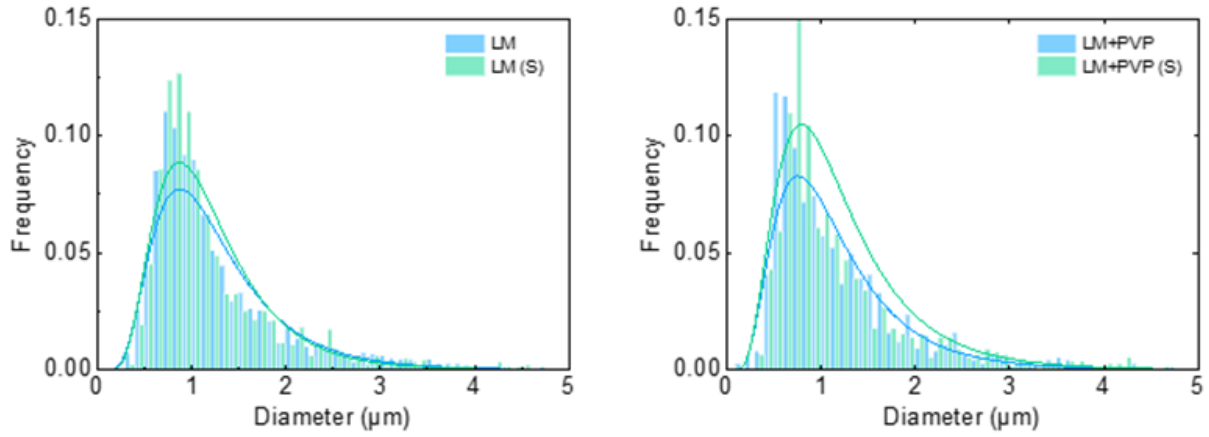

Figure 23 Comparison of the size distribution of EGaIn particle in different material combinations (EGaIn & EGaIn + PVP)

Next, we turn to Figure 22 which displays a comparison of the particle size distributions before and after shear mixing for two systems: EGaIn + Ecoflex with and without PVP. Upon examination of these two particle size distribution curves, we observe that the left curve, representing the EGaIn + Ecoflex system without PVP, exhibits a higher peak value and a rightward shift after shear mixing. On the other hand, the right curve, corresponding to the EGaIn + Ecoflex system with PVP, displays a more pronounced decrease in peak value and a greater rightward shift. Comparing the particle size data from the left curve, we observe that the mean particle sizes before shear mixing are 1.278 and 1.368 (S) μm, and after shear mixing, the mean particle size significantly increases, indicating that the addition of Ecoflex may have an impact on the particle size. The median particle sizes are 1.04 and 1.095 (S) μm, respectively. Turning to the particle size data on the right plot, we observe that the mean particle sizes before shear mixing are 1.17 and 1.446 (S)

μm, respectively, and that the mean particle size increases noticeably. The median particle sizes are 0.944 and 1.124 (S) μm, respectively.

Based on these data, we can draw the preliminary conclusion that the addition of Ecoflex leads to an increase in particle size. Moreover, the increase is more pronounced in the case of the EGaIn + Ecoflex system with PVP. Even when comparing the particle size distributions after shear mixing, the mean particle sizes for EGaIn + PVP and the system with all three components are 1.237 and 1.446 (S) μm, respectively, while the median particle sizes are 0.944 and 1.124 (S) μm, respectively. The reason for this increase in particle size could be explained by the aggregation of EGaIn particles. Since the sonication decreases the particle size, high surface energy of EGaIn particles can lead to instability. To suppress this energy, increasing the size of EGaIn particles is the easiest way. The shear mixing process just provides a driving force to enlarge the particles, which results in aggregation.

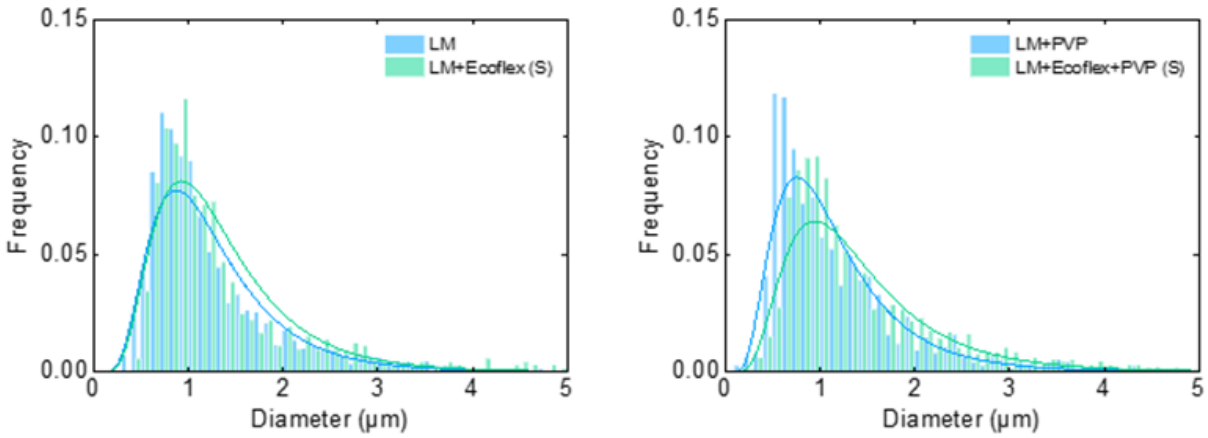

Figure 24 Comparison of the size distribution of EGaIn particle in different material combinations (EGaIn + Ecoflex & EGaIn + Ecoflex + PVP)

Figure 23 shows the box plots for six cases, where blue and green represent samples without and with shear mixing, respectively. This figure clearly shows that EGaIn + PVP + Ecoflex has the largest particle size, in terms of both mean and median values. However, the difference in particle size is not significant.

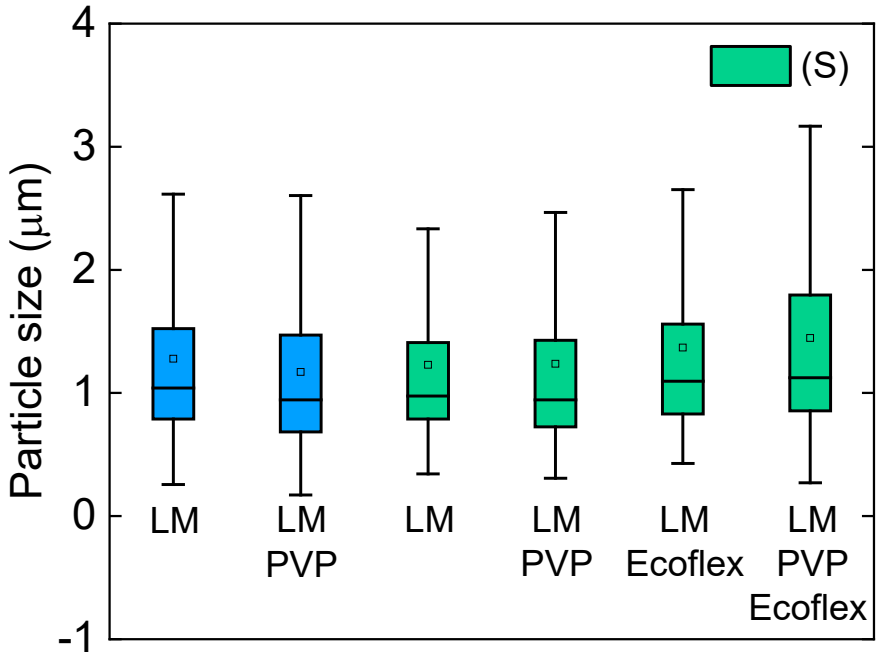

Figure 25 Box plot of EGaIn particle in different material combinations, tiny square and middle bar are mean and median value, respectively

5.2.6. Particle Size Distribution Analysis – 2nd

To verify the accuracy of the experiments, the particle size distribution was analyzed again using the same method. Six different situations were examined using three materials, but this time, the particle size distribution was determined using both the micrographs and SEM images. The higher resolution of SEM allowed for clearer imaging of smaller particles, and it was anticipated that the second round of particle size analysis would be more informative.

Figure 24 presents a comparison of the particle size distribution before and after shear mixing for pure EGaIn and EGaIn + PVP, shown on the left and right sides, respectively. The particle size changes after shear mixing were found to be negligible, with results that were almost identical to the previous analysis. For the pure EGaIn sample, the average particle size was found to be 1.937 μm and 1.904(S) μm before and after shear mixing, respectively. The average particle size decreased after shear mixing, and the trend was consistent with the previous analysis. However, the overall particle size was found to be larger in this analysis, with median particle sizes of 1.226

μm and 1.278(S) μm before and after shear mixing, respectively. For the EGaIn + PVP sample, the average particle size was the same, at 1.684 μm, while the median particle sizes were 0.977 μm and 0.901(S) μm, respectively. The results of the first half of the analysis were similar to those of the first experiment, indicating the reliability of this particle size analysis.

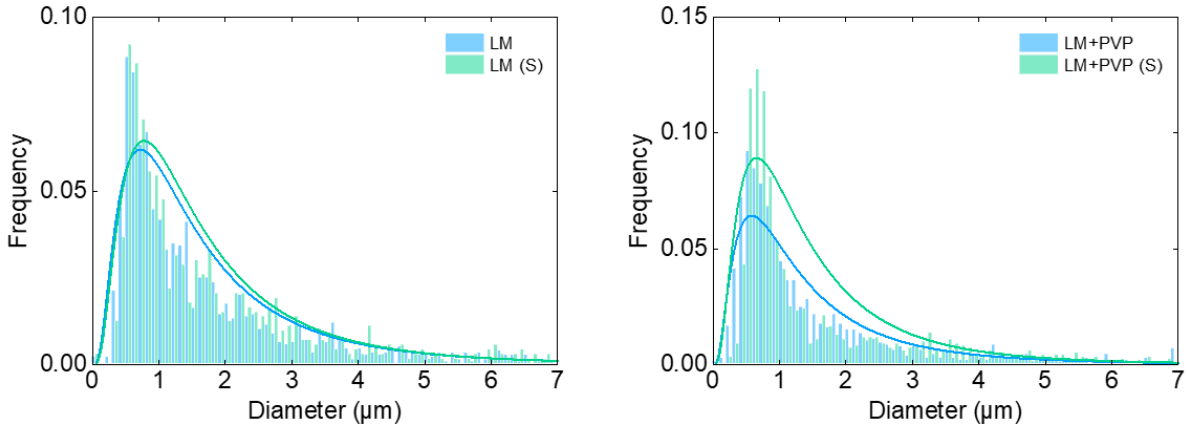

Figure 26 Comparison of the size distribution of EGaIn particle in different material combinations (EGaIn & EGaIn + PVP), 2nd time

Next, we have Figure 25 which displays a comparison of particle size distribution before and after shear mixing for EGaIn + Ecoflex and EGaIn + Ecoflex + PVP, respectively. The particle size distribution plot on the left shows a higher peak after Ecoflex shear mixing, while the peak position remains almost unchanged. On the other hand, the plot on the right shows a significant decrease in peak height and a substantial rightward shift of the peak, revealing the tendency for larger particles to become even larger. The analysis of the particle size data on the left plot shows that the mean particle sizes before and after shear mixing are 1.937 and 1.828(S) μm, respectively. The results clearly indicate that the addition of Ecoflex may affect the particle size, and the median particle sizes are 1.226 and 1.073(S) μm, respectively. Turning to the analysis of the particle size data on the right for the LMEC, the mean particle sizes before and after shear mixing are 1.684 and 1.743(S) μm, respectively. The average particle size increases significantly, and the median particle sizes are 0.977 and 1.357(S) μm, respectively. The difference in the median particle size is the largest observed in these experiments and 1.357 μm is also the largest among all median particle sizes.

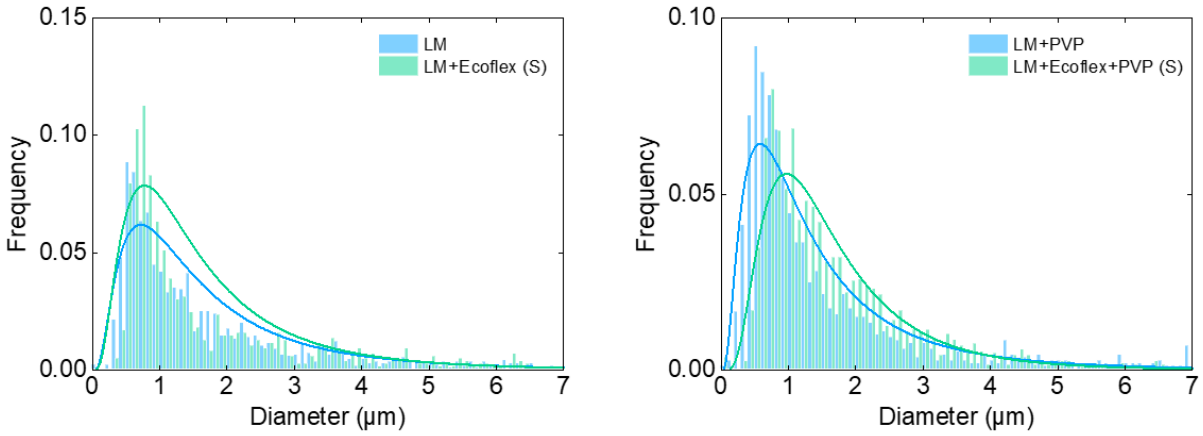

Figure 27 Comparison of the size distribution of EGaIn particle in different material combinations (EGaIn + Ecoflex & EGaIn + Ecoflex + PVP), 2nd time

Finally, let's look at the box plot for the second particle size experiment. As shown in Figure 26, although the overall particle size is slightly larger than the previous experiment, the results are somewhat similar, and the differences are not significant. EGaIn + PVP + Ecoflex still has the largest median particle size. In fact, the particle size differences among the six different conditions are quite small, indicating that the increase in particle size due to shear mixing is not a measurement error but also does not significantly affect the experiment.

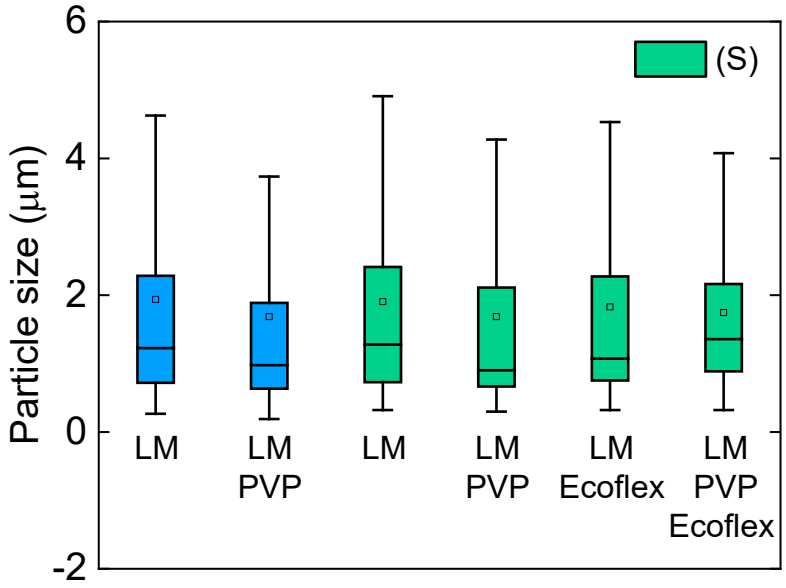

Figure 28 Box plot of EGaIn particle in different material combinations, tiny square and middle bar are mean and median value, respectively, 2nd time

Combining the results of the two particle size analyses, we can conclude that the addition of both Ecoflex and PVP with shear mixing can cause an increase in the size of EGaIn particles. While this change in size is not significant enough to alter the strain-activation or conductivity, it is still noteworthy. Similarly, Crater et al.[47] recently reported that the particle size of liquid metals increases after being introduced into composites, indicating that the phenomenon we observed is not a coincidence. Additionally, the first analysis showed that adding Ecoflex increased particle size, while the second analysis showed a decrease in size. This suggests that Ecoflex may have a role in altering particle size, though the mechanism behind these two changes is still unknown and requires further experimentation and analysis for a better understanding.

5.3. Electromechanical Measurements

The mechanical-electrical properties have always been the most important aspect of stretchable electronics. This chapter includes the electrical conductivity at activation, maximum strain, and different displacement rates, at uniaxial tensile strain. As a definition, the resistance variation (ΔR) is the difference between the resistance (R) and the initial resistance (R_0), that is, $\Delta R = R - R0$. ΔR is then divided by R_0 to obtain the percentage of the resistance variation.

5.3.1. Investigation of Electrical Properties during Activation Process

The specific activation process has been identified by measuring resistance, as shown in Figure 27. First discuss the 1 mm/sec slow displacement rate activation. The reason for no numerical changes before 200% strain is that resistance was not measured until then. Resistance started to decrease at 200% strain and continued to drop to 350% strain, exhibiting stable values. Many interesting phenomena were observed during the process. Firstly, resistance decreased in a stepwise rather than linear or curved pattern, indicating that the activation process was not gradual. Secondly, although activation began at 200% strain, a significant drop in resistance did not occur until 290% strain, indicating that 300% strain was the key to activation for slow displacement rate.

Next, we investigate the effect of a fast displacement rate of 25 mm/sec on activation. By observing the two activation curves in Figure 27, we can see that different activation rates produce vastly different results. The light blue activation curve experiences a sharp decrease in resistance at 100% strain, followed by a slow decrease to below 1 Ω/cm. The difference in results here may be due to differences in the efficiency of oxide shell rupture caused by the rate difference. When the activation rate is slower, the EGaIn particles have enough time to undergo slight displacement, which delays the activation process as the shear force cannot break the oxide shell immediately. On the other hand, when the activation rate is faster, the EGaIn particles do not have time to be displaced, and the shear force acts entirely on the oxide shell, leading to a faster activation as the oxide shell is ruptured more efficiently. As for the different initial resistances observed in the samples after activation, especially the significantly higher initial resistance at lower activation rates, the experiments confirm that this phenomenon is irreversible and cannot be reduced by re-stretching, indicating that low activation rates cause a decrease in the conductivity of the conductive pathway.

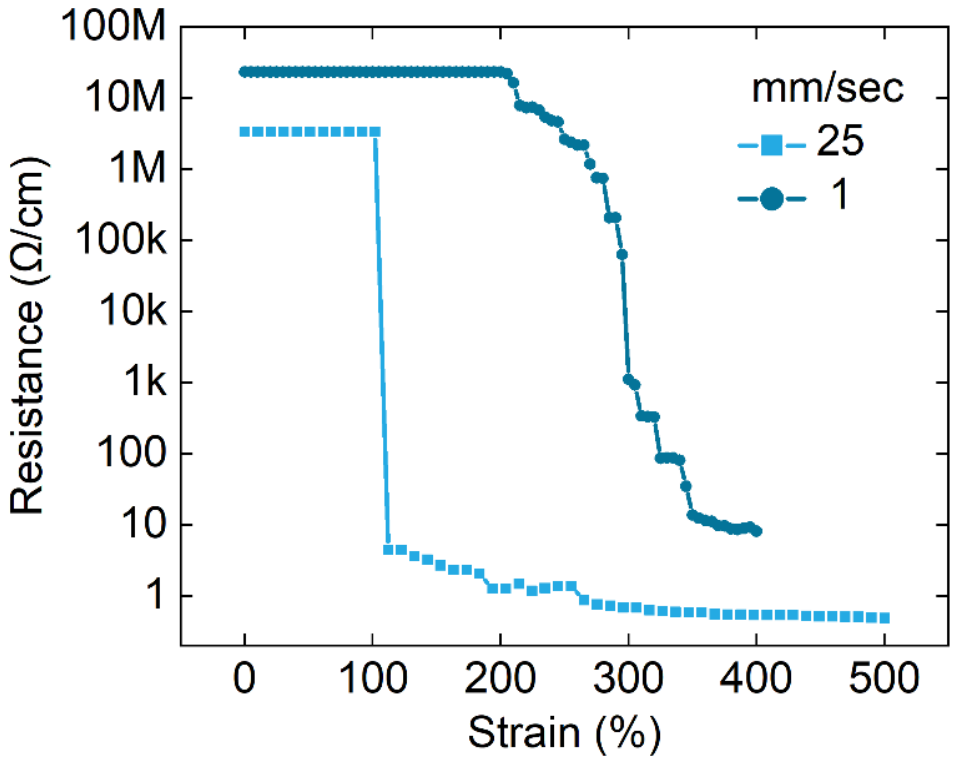

Figure 29 Electrical resistance of the strain-activation process at different displacement rate as a function of strain

In Figure 28, images before and after activation were compared, and it was found that the conductive pathway did not experience damage but only a color change. The conductive pathway did not break into sections during stretching, demonstrating that it has high stretchability. Through our testing, it was found that stretching at least five times and shortening the stretching time can result in more uniform activation of the conductive pathway.

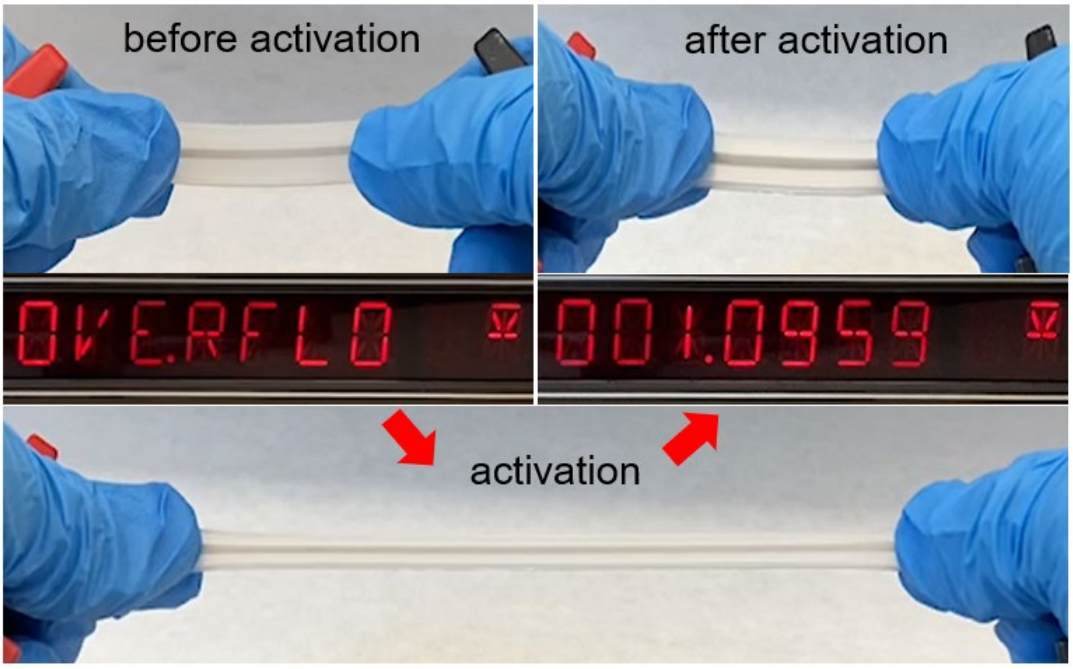

Figure 30 Illustration of strain-activation process

5.3.2. Measurements of High Strain Resistance and Conductivity

The maximum strain has always been a popular topic when discussing stretchable electronics. In general, the higher the better. Therefore, we measured the maximum strain and the change in electrical resistance of LMEC under strain. As shown in Figure 30, the conductive pathway after activation achieved an ultra-high stretchability of 700% strain. This value is extremely impressive because the strain level represents its application range, and 700% strain indicates that this LMEC can be stretched up to 7 times its original length, making it suitable for almost any deformation application. Moreover, even at 700% strain, the resistance variation is still less than 100% of its original value (92.4%). For this sample, the initial resistance was 0.328 Ω/cm, and even if the resistance variation increased to 100%, the resistance would only increase to 0.656 Ω/cm, well within the acceptable range. Compared with the ideal curve drawn in the upper left corner of Figure 29 using Pouillet's Law, the resistance variation is almost negligible. Therefore, it can be boldly stated that this LMEC is very promising, especially in the field of mechatronics, and can be applied in numerous stretchable electronic and wearable devices.

Figure 30 shows the actual displacement photo, and it can be found that there is no defect such as breakage or fracture during the stretching process.

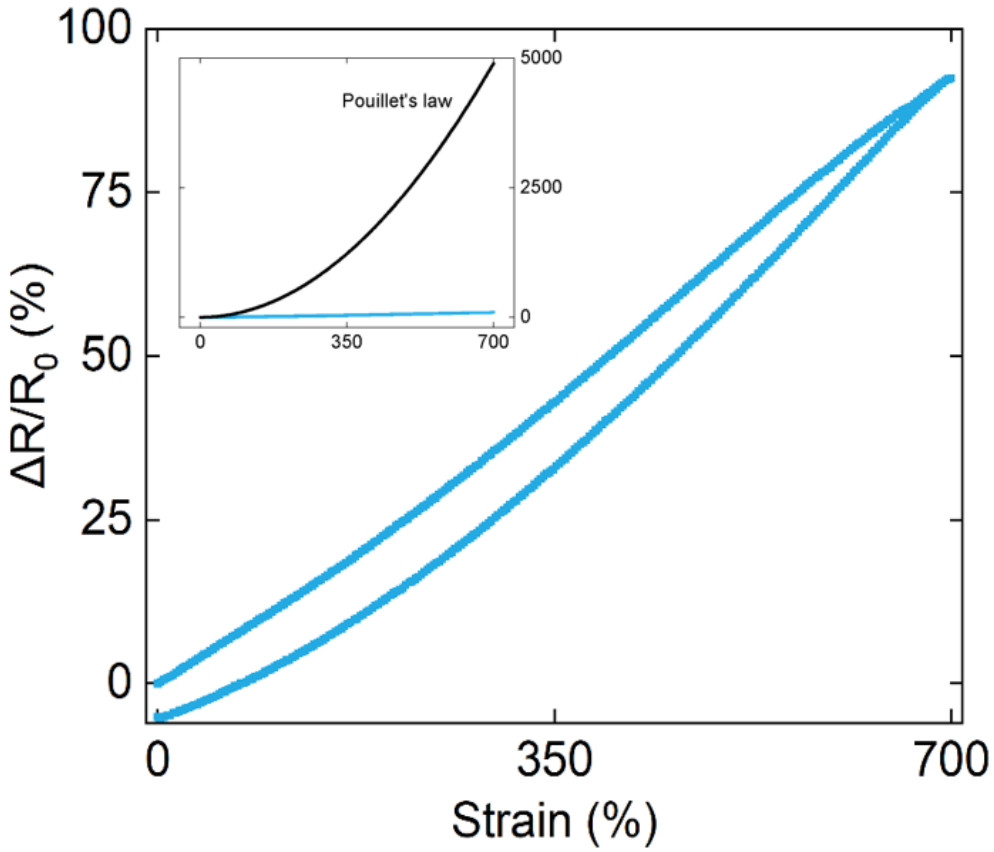

Figure 31 Electrical resistance variation of the activated sample as a function of strain

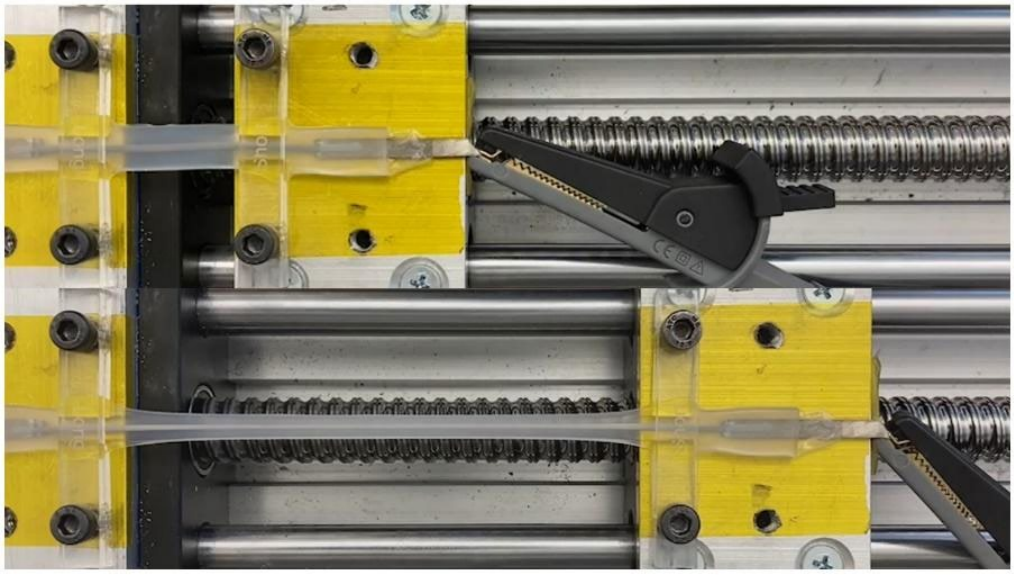

Figure 32 Photographs of LMEC during tensile loading up to 700% strain

5.3.3. Electromechanical Properties of Different Weight Ratios of Ecoflex Synthetic Units A and B

As the discussion in Chapter 5.1.12, conductive pathways with different weight ratios of Ecoflex synthetic units A and B had similar results of electrical resistance. Since the electrical properties were confirmed, we also conducted electromechanical experiments. Figure 31 shown the resistance variation between the two extreme ratios of 9:1 and 1:9 as strain varies. Clearly, both exhibit excellent tensile strength, and were stable up to 400% strain. At the same time, the minimal resistance variation demonstrates remarkable conductivity, which was more significant than the theoretical value of Pouillet's law in the top left corner plot. However, the resistance of 9:1 and 1:9 varied more at 300% strain with 22.65% and 19.72%, respectively, compared to the 1:1 ratio sample, 13.92%. This means that when the ratio is not 1:1, the electromechanical properties will still be affected. This electromechanical test illustrated that the ratio of Ecoflex synthetic units is not as important as expected, even if it is not added in equal proportions, it will only slightly affect some mechanical properties.

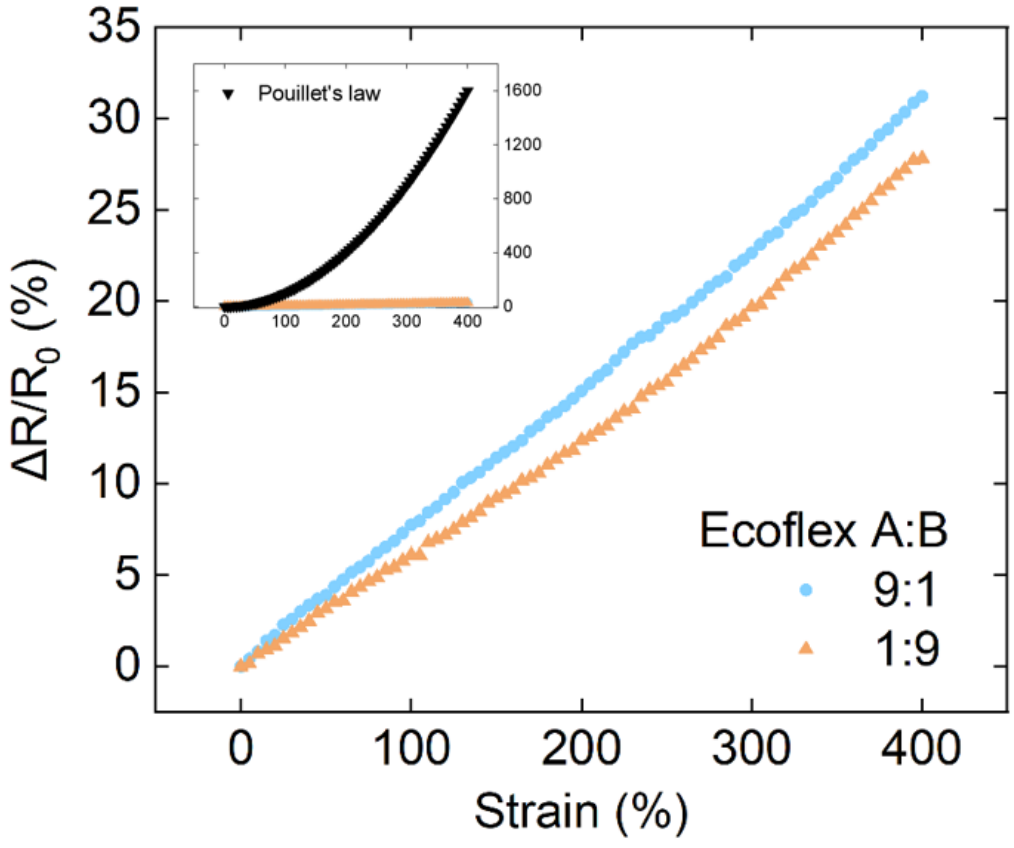

Figure 33 Electrical resistance variation of the activated samples as a function of strain with different ratios, Ecoflex part A and B

5.4. Exploration of Displacement Rate

Here, we try to answer the third question of this study, "Does the electromechanical response of LM-based conductors depend on the rate of applied deformation?". To answer this, we measured different displacement rates and their electrical properties, and investigated the relationship between them. Two cases were tested, the maximum resistance variation caused by different displacement rates in a single cycle with a strain from 50% to 300%, and the maximum resistance variation caused by different displacement rates in five cycles with a fixed strain of 200%. It should be noted that the maximum resistance variation is obtained by subtracting the minimum value from the maximum value of the resistance variation ($(R-R_0)/R_0$). By introducing the concept of maximum resistance variation, we can simplify the resistance variation of a single cycle into a percentage. Comparing the magnitude of the maximum resistance variation, the relationship between the electrical stability and the different shift rates can be better interpreted.

5.4.1. Maximum Resistance variation Caused by Different Displacement Rates in a Single Cycle

For electronic stretching, different strains correspond to different conductive responses. However, there is no previous study that shows the electromechanical response at different displacement rates. Therefore, we observed the results of different displacement rates under different uniaxial strains. As mentioned in the previous paragraph, we used a commonly used strain range of 50% to 300%. The displacement rate is also adopted from 0.1, 0.25 mm/sec, which is commonly used in general tensile testing, to 20 mm/sec, which is close to the displacement rate limit of the instrument we use. Also, only one stretching cycle is measured for each condition.

Figure 32 shows the differences in resistance at different displacement rates under strains ranging from 100% to 300%, from left to right. Among the many curves, the light blue and dark blue curves are the most prominent, representing displacement rates of 0.1 and 0.25 mm/sec, respectively, and show somewhat different results from other rates. The curves for 0.1 and 0.25 mm/sec exhibit non-linear trends, especially 0.1 mm/sec, which has a higher resistance variation at low strains compared to other rates, but the opposite is true at high strains. The curves for the other displacement rates, besides exhibiting a linear trend, also show that resistance variation is generally inversely proportional to the rate, i.e., the faster the rate, the smaller the resistance variation. Furthermore, these curves for the other rates are all very stable, with almost no difference between the stretching and returning processes, even when the strain reaches 300%, with a resistance variation of less than 15%.

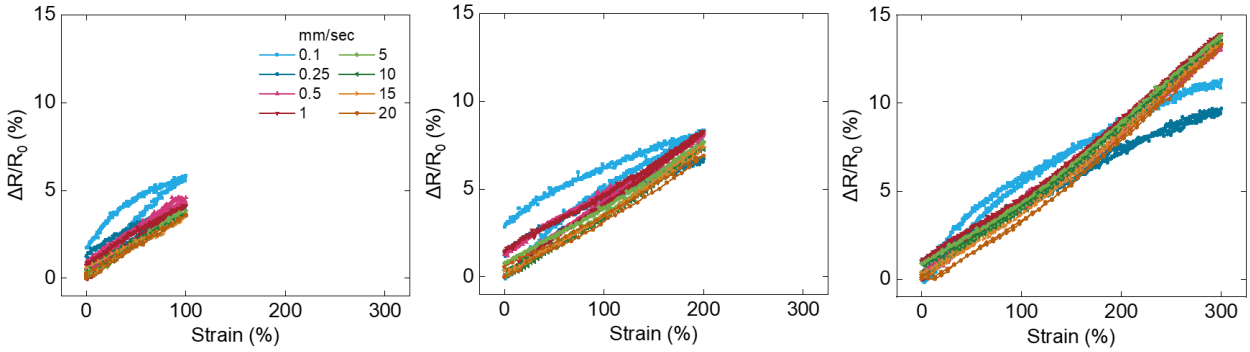

Figure 34 Electrical resistance variation of the activated samples as a function of strain with different ratios,

After examining the effects of strain on resistance variations at different displacement rates, let us now explore the effects of strain on resistance variations at the same displacement rates. Figure 33 illustrates the results of three displacement rates, from left to right: 0.1, 1, and 20 mm/sec. The first two displacement rates are commonly used in many studies, and they exhibit distinctly different resistance variations. Similar to what was mentioned in the previous paragraph, a saturation phenomenon is observed at higher strains for the 0.1 mm/sec curve. If we closely examine the left graph of Figure 33, the brown curve corresponds to 50% strain, where there is no apparent saturation phenomenon. However, as we move to the orange curve (100% strain), a clear saturation phenomenon occurs, indicating that there is insufficient time for percolation to reach other regions when the strain is extremely low.

The middle plot of Figure 33 corresponds to a displacement rate of 1 mm/sec, which shows a linear trend without saturation phenomenon. At 300% strain, the resistance variation is 13.92%, and the stretching and returning paths do not completely overlap at every strain but are still highly stable. The right panel of Figure 33 corresponds to a displacement rate of 20 mm/sec and also shows a linear trend. At 300% strain, the resistance variation is 13.28%, and the stretching and returning paths almost completely overlap and are highly stable. Comparing the middle and right panels, higher displacement rates lead to lower resistance variations, which is consistent with the previous chapter. Therefore, for large-scale stretching applications of this LMEC, a higher displacement rate will provide more stable and lower resistance variations.

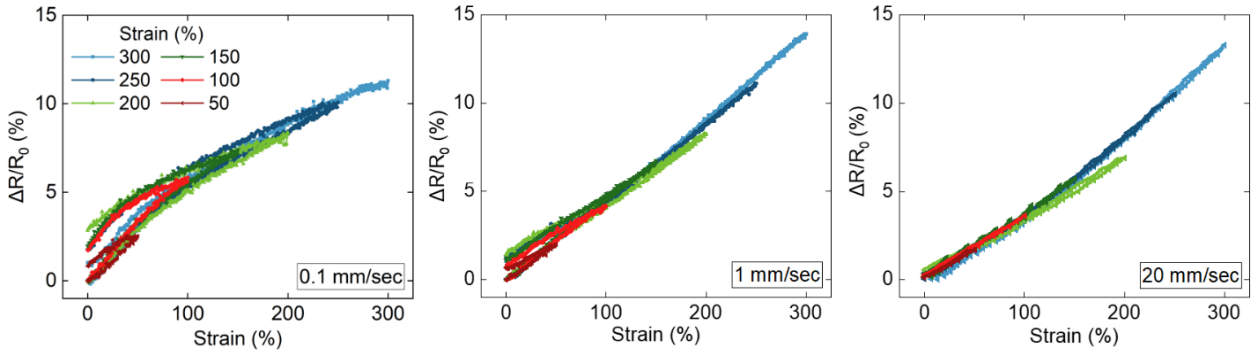

Figure 35 Electrical resistance variation of the activated samples as a function of strain with different ratios, Ecoflex part A and B

Finally, we come to the section heading "Maximum Resistance variation". This resistance variation is simply the difference between the maximum and minimum values, so there is only one value per 50% strain, which effectively simplifies our results. Figure 34 shows the effect of strain on the maximum resistance variation under different displacement rates. Despite the data simplification, the results are still very similar to those of the right graph in Figure 32, since the strain range is the same. Generally, all displacement rates exhibit a positive correlation in a left-down-to-right-up direction, with rates of 0.1 and 0.25 mm/sec showing a lower maximum resistance variation at 300% strain. If we ignore rates of 0.1 and 0.25 mm/sec and fit a trend line to this graph, we obtain a straight line with a slope of 0.046. This positive correlation line can be used to design applications such as detecting strain based on resistance variation when a specific resistance value is detected, and vice versa.

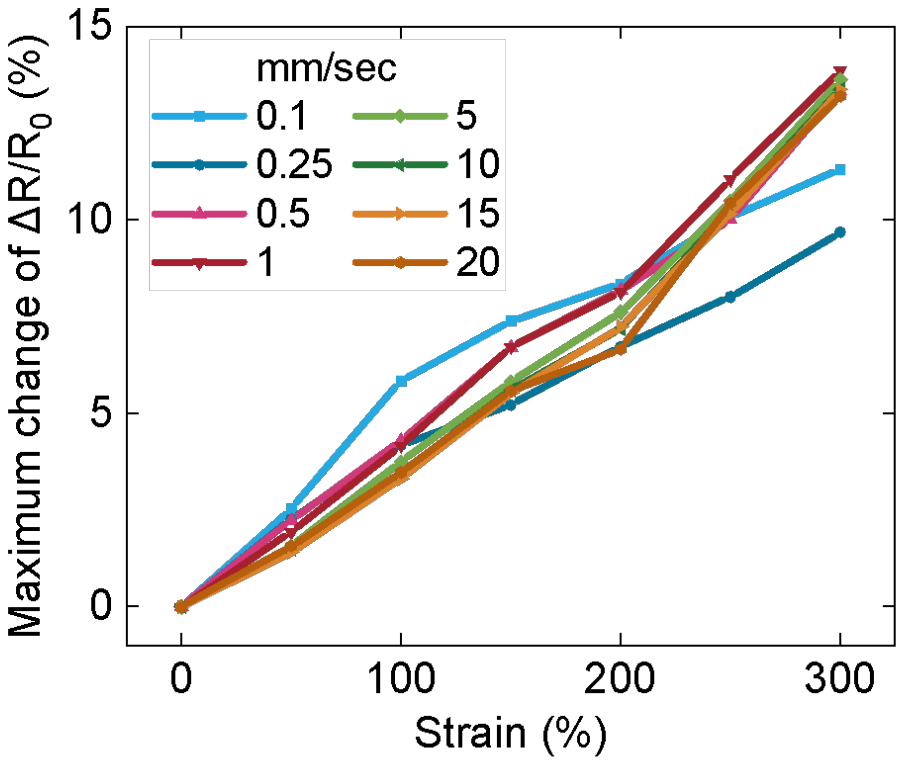

Figure 36 Maximum change of electrical resistance variation of the activated samples as a function of strain with different displacement rates

5.4.2. Maximum Resistance variation Caused by Different Displacement Rates in five cycles

The previous chapter discussed the resistance variation under single tensile cycle, while this chapter raises the number of tensile cycles to five to observe whether multiple tensile cycles will affect stability and resistance variation. Figure 35 shows the influence of different displacement rates on resistance variation under 200% strain. As mentioned in the previous chapter, low displacement rates have lower resistance variations than high rates at high strains (such as 300%), but still have higher resistance variations at 200% strain. Therefore, we can see that the light blue curve in Figure 35, representing 0.1 mm/sec, has the highest resistance variation (12.84%). As the displacement rate increases, the resistance variation tends to decrease, which is similar to that of single tensile cycle.

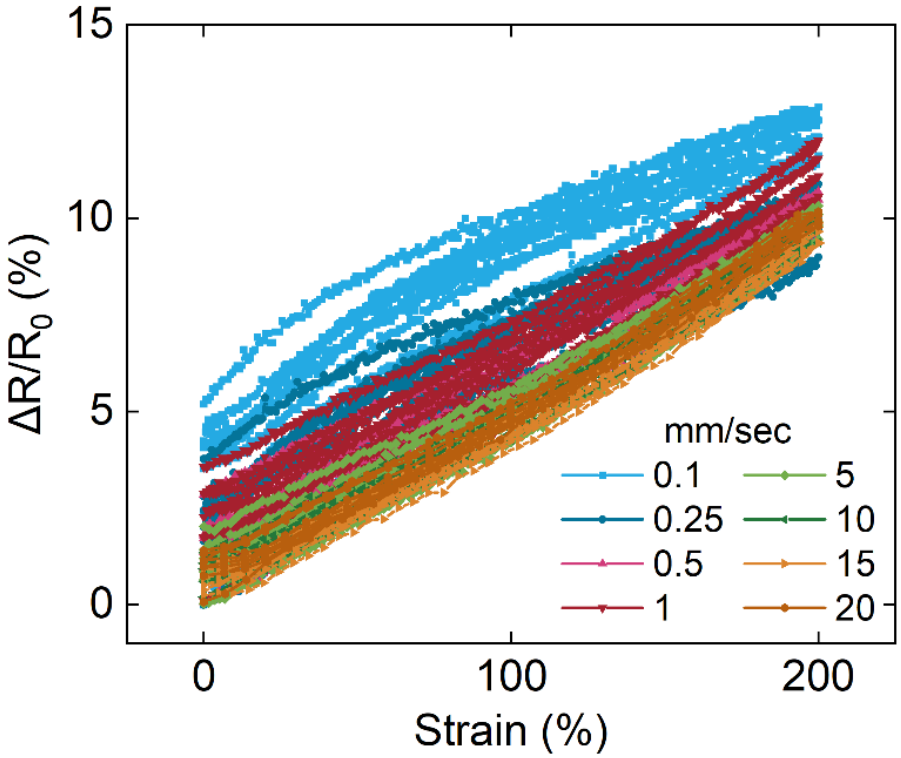

Figure 37 Electrical resistance variation of the activated samples as a function of strain with different displacement rates, five cycles

However, if we plot each displacement rate separately, as shown in Figure 36, we will have different findings. The numbers above each graph represent the displacement rate used in the test. Interestingly, low displacement rates, such as 0.1 to 1 mm/sec, have a larger plotting area compared to high rates. As all curves start from (0,0), the larger plotting area indicates unstable resistance variations and a trend of increasing resistance variations. Among them, the 0.1 mm/sec has the largest difference, with up to 3% variation between different cycles. This result highlights the issue of low displacement rates, which although may result in less resistance variation in single tensile cycle, perform poorly in practical applications, which involve multiple cycles of tension.

On the contrary, if we consider the displacement rates of 5 to 20 mm/sec as high rates, then there is very little difference between the cycles. Especially, 10 to 20 mm/sec shows very stable electromechanical properties, and the resistance variation between different cycles is less than 1%. Moreover, the resistance variation under high rates performs almost identically, and the values after five stretching cycles are very close. Interestingly, whether it is a single cycle or multiple

cycles, the resistance variation at 15 mm/sec is always lower than that at 20 mm/sec. The resistance variation at 15 mm/sec is also the lowest among all rates, indicating that this is the optimal displacement rate for this LMEC.

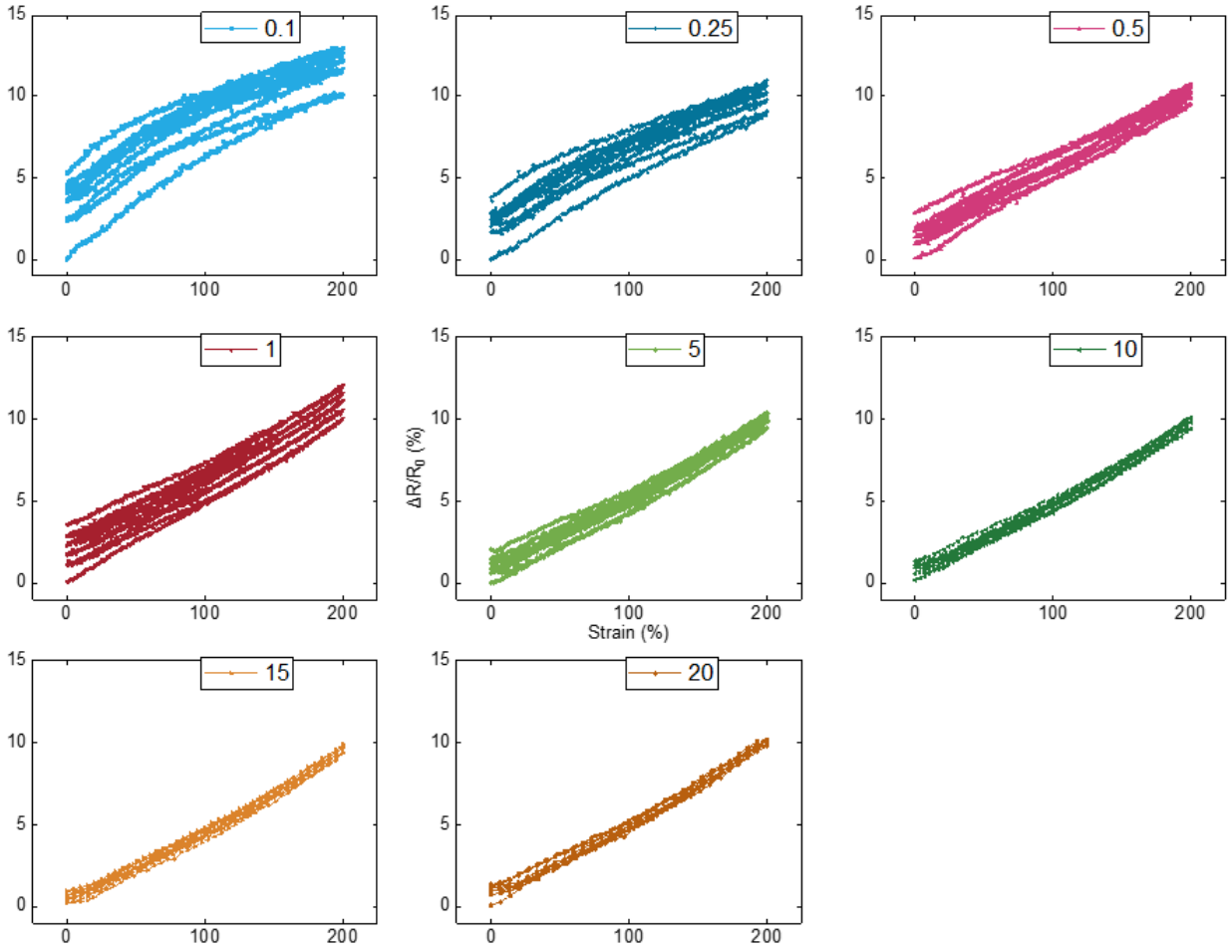

Figure 38 Electrical resistance variation of the activated samples as a function of strain with different displacement rates, five cycles, individual display

In the same vein as the previous section, we will examine the maximum resistance variation in this section. As each displacement rate underwent five tensile cycles, we plotted an error bar graph (Figure 37) to investigate the effect of different rates on the maximum resistance variation. It is evident that lower displacement rates result in smaller maximum resistance variations, particularly when the rate is below 1 mm/sec. Overall, all maximum resistance variations were around 9%, with the lowest difference at 8.3% for 0.25 mm/sec. Upon closer inspection of Figure 37, the absence of error bars for 10 and 15 mm/sec implies minimal variations in maximum resistance variations across different tensile cycles, indicating the extremely stable

electromechanical properties of the LMEC. Through multiple tensile cycle testing, it can be concluded that this composite material exhibits exceptional stability in electromechanical behavior and performs well in both single and multiple cycles.

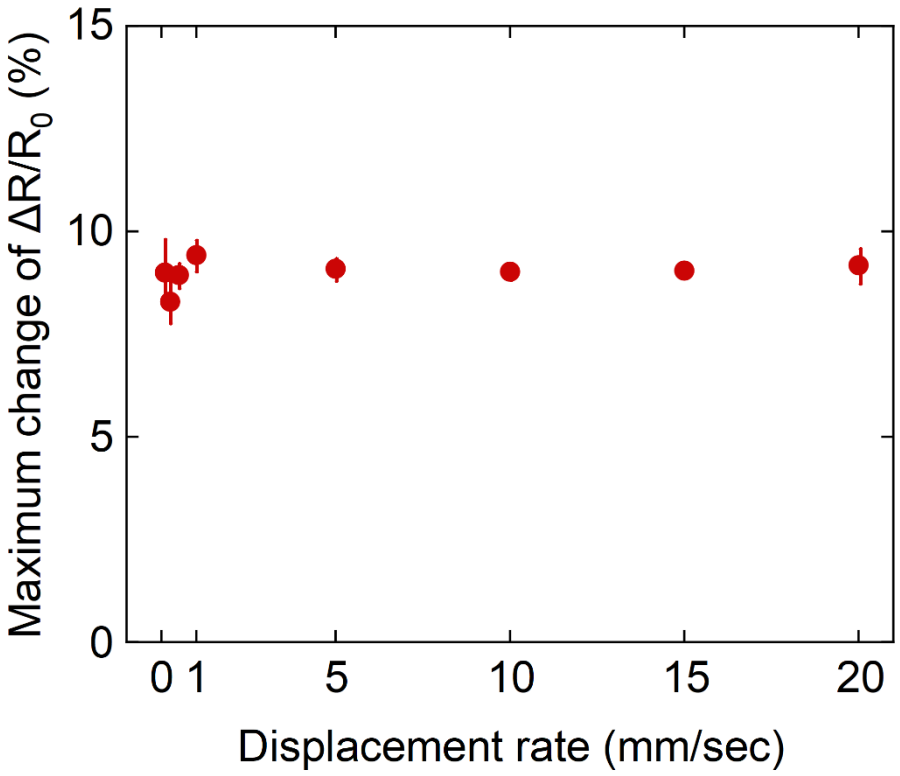

Figure 39 Maximum change of electrical resistance variation of the activated samples as a function of displacement rates

5.4.3. Comparative Study of Exploration of Displacement Rate of LMEC and Sprayed EGaIn

To demonstrate the excellent electromechanical properties of our created LMEC, we require a material with a similar property for comparison through cyclic stretching. We have found that Sprayed EGaIn is an excellent candidate since it is a liquid metal-based conductor. Firstly, the manufacturing process of sprayed EGaIn is straightforward, requiring only the pre-measurement of the area to be sprayed. For example, as shown in Figure 38, the conductive pathway area was 50×2.3 mm^2, and the mask/stencil of the same area was cut and placed on the Ecoflex substrate to create a conductive pathway similar to LMEC. Furthermore, this type of sprayed EGaIn retains its conductivity even after stretching and does not require activation (original electrical resistance is 0.3 Ω/cm).

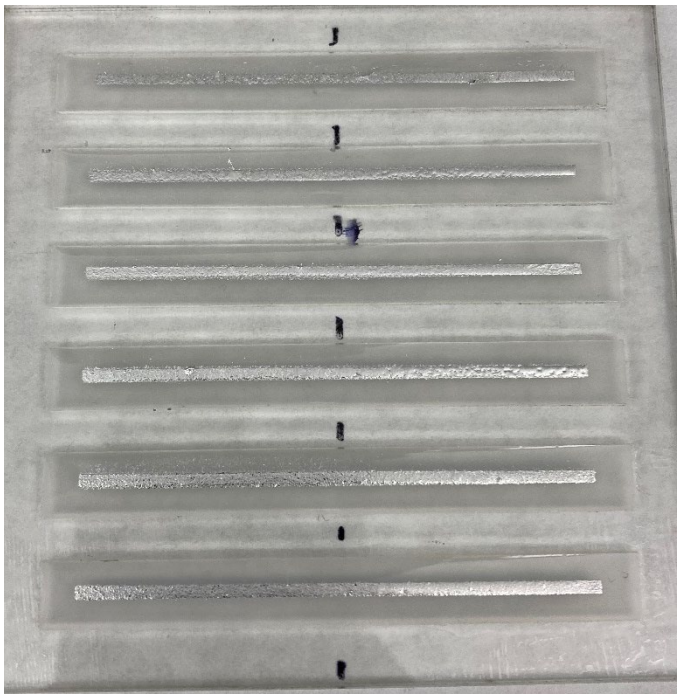

Figure 40 Fabrication illustration of sprayed EGaIn

5.4.4. Sprayed EGaIn: Maximum Resistance variation Caused by Different Displacement Rates in a Single Cycle

To compare with the LMEC, we followed the same method to investigate if Sprayed EGaIn exhibits different trends. Figure 39 shows the resistance variation at different displacement rates from 100% to 300% strain. It can be observed that there is no significant difference among different rates when the strain is less than 100%. It is worth noting that the resistance variation between the lowest displacement rate of 0.1 mm/sec and the highest rate of 20 mm/sec is close to 6%, which are 7.08% and 12.66%, respectively. When the strain is less than 200%, the light blue curve of the rate of 0.1 mm/sec and dark bule curve of the rate of 0.25 mm/sec show completely different trends from the other rates. While the other rates show steeper slopes, the two lower rates exhibit smoother slopes with lower resistance variation. Finally, when the strain is within 300%, almost all of the displacement rates exhibit a close-to-linear relationship and the highest and lowest resistance variation are 66.4% and 57.8%, respectively.

Upon careful observation, it can be noted that when stretched and returned to the starting point at a lower rate, the difference in resistance is mostly negative, indicating a decrease in resistance after stretching, similar to strain-activation. The reason for the decrease in resistance is still unknown, but it might be similar to the explanation provided in the previous chapter, where slow stretching

causes EGaIn to fully percolate into the conductive pathway, resulting in both the maximum decrease in resistance variation and in zero-strain resistance.

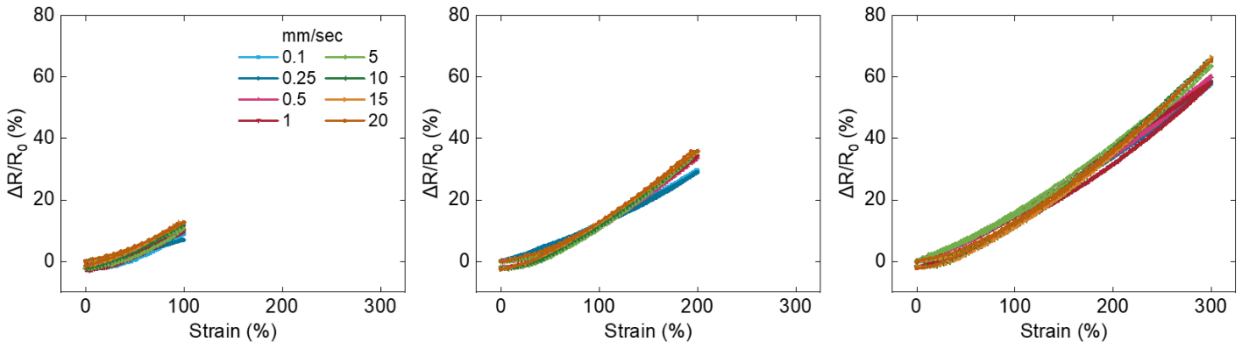

Figure 41 Electrical resistance variation of sprayed EGaIn samples as a function of strain with different displacement rates

After examining the effect of strain at different displacement rates on resistance variations, let us now take a look at the effect of strain at the same displacement rate on resistance variations. Figure 40 shows the results for three different displacement rates, from left to right: 0.1, 1, and 20 mm/sec. Starting with 0.1 mm/sec, as previously mentioned, the sprayed EGaIn showed unstable stretching and returning cycles at low displacement rates. However, unlike the saturation trend observed in LMEC, the trend of sprayed EGaIn at low rates is linear. Meanwhile, at 300% strain, non-overlapping stretching and returning curves also appeared. At 1 mm/sec, non-overlapping stretching and returning cycles also appeared at 300% strain, while the resistance remained relatively stable at other strains. At 20 mm/sec, the resistance remained linear and stable, with little change from 50% to 300% strain. However, although it remained stable, its highest resistance variation reached 66.4%, which is much higher than the highest resistance variation of 57.8% at 0.1 mm/sec.

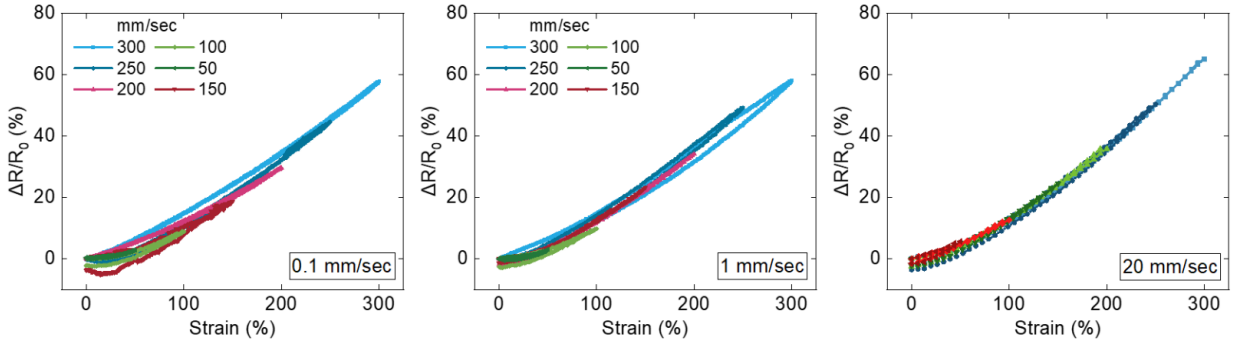

Figure 42 Electrical resistance variation of sprayed EGaIn samples as a function of strain with specific displacement rates

The Figure 41 shows the effect of strain on the maximum resistance variation under different displacement rates. In general, there is a linear relationship from bottom left to top right, with maximum and minimum resistance variations of 66.4% and 57.8%, respectively. Similar to Figure 34, low displacement rates such as 0.1 mm/sec resulted in relatively lower maximum resistance variations at 300% high strain. Under high displacement rates, both the LMEC and sprayed EGaIn showed stable increases in maximum resistance variation. Overall, although sprayed EGaIn's maximum resistance variation is slightly higher, its performance in a single tensile cycle is still impressive.

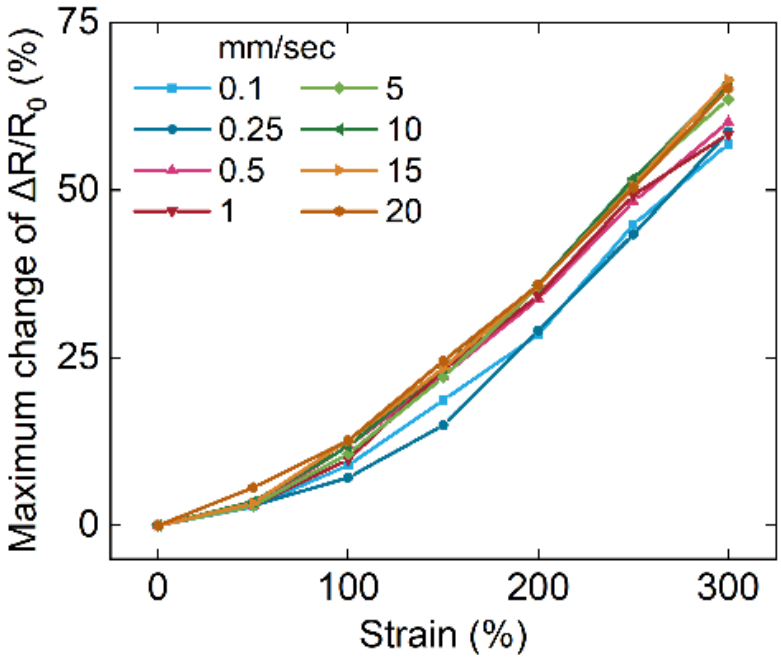

Figure 43 Maximum change of electrical resistance variation of sprayed EGaIn samples as a function of strain with different displacement rates

5.4.5. Sprayed EGaIn: Maximum Resistance variation Caused by Different Displacement Rates in Five Cycles

We also investigated the resistance response of sprayed EGaIn under multiple stretching cycles. All measurement conditions were consistent with the previous study to ensure the accuracy of comparison. Figure 42 shows the effect of strain on resistance variations at different displacement rates for five stretching cycles. It can be observed that the differences between different cycles are small, and the resistance variations between different rates are all concentrated between 27% and 32%, indicating good stability overall. Interestingly, at 200% strain, the maximum and minimum

resistance variations were 32.42% for 5 mm/sec and 27.65% for 0.25 mm/sec, respectively, coming from the first and last cycle.

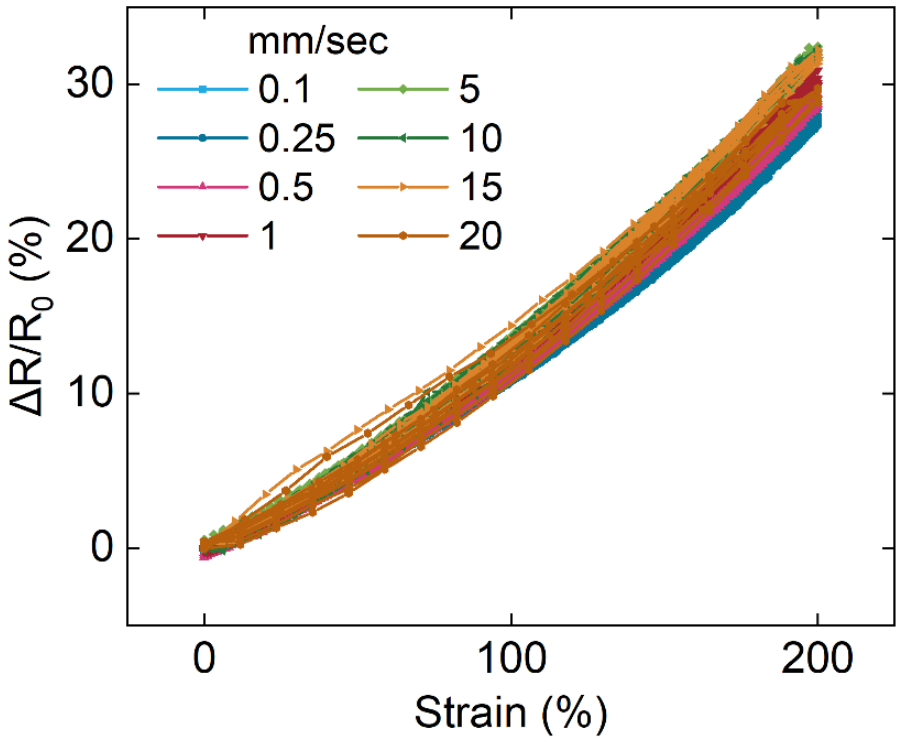

Figure 44 Electrical resistance variation of sprayed EGaIn samples as a function of strain with different displacement rates, five cycles

We plotted the eight displacement speeds separately in Figure 43. It can be observed from this figure that there are no significant differences in sprayed EGaIn performance at different speeds. Except for a slight deviation in the first cycle for 15 and 20 mm/sec, the results are almost identical to those of a single cycle. The differences between different cycles are small, and the stability is high, making it suitable for repeated stretching. The only difference between sprayed EGaIn and LMEC is that the change in resistance is larger in sprayed EGaIn, which means the conductivity at high strain tend to decrease more.

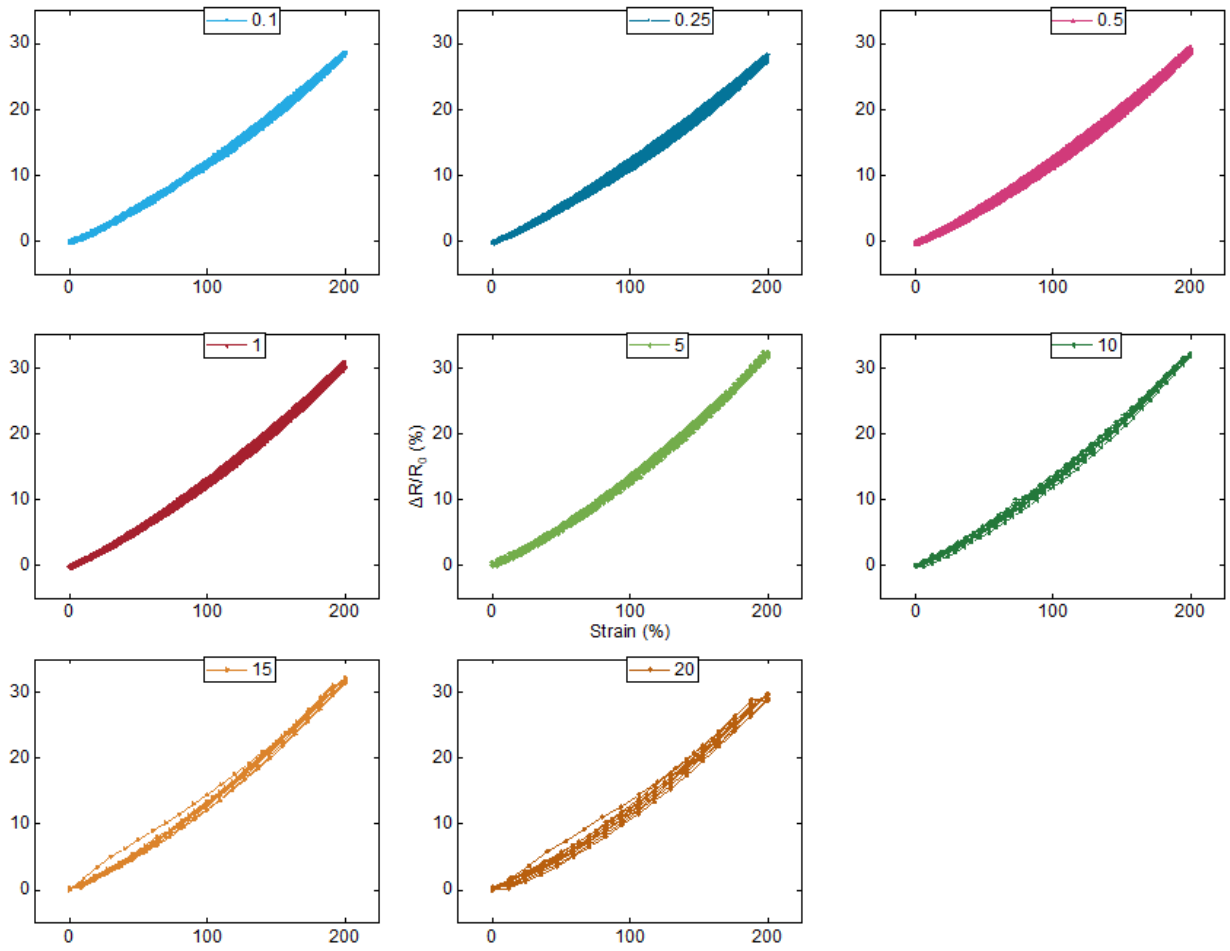

Figure 45 Electrical resistance variation of sprayed EGaIn samples as a function of strain with different displacement rates, five cycles, individual display

The calculated maximum resistance variations are plotted against displacement rate in Figure 44. All the maximum resistance variations are around 30%. Low displacement rates exhibit lower resistance variations similar to the behavior of LMEC, and the threshold is still 1 mm/sec. Although the differences are small, it still proves that low displacement rates have lower resistance variations than high rates. Considering the high stability under multiple cycles, sprayed EGaIn may be more suitable for tensile tests at low displacement rates.

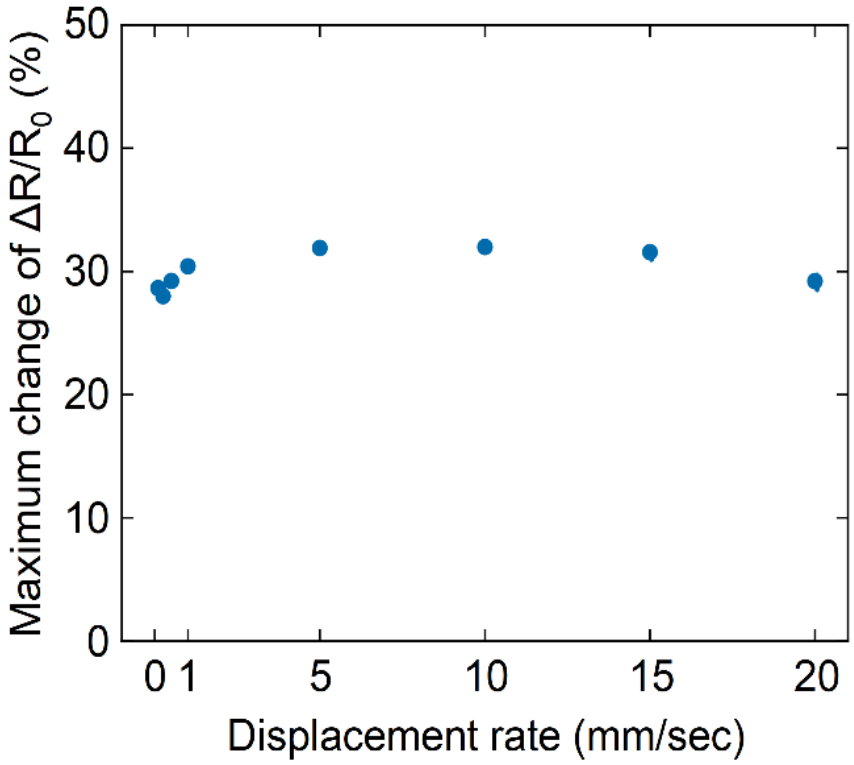

Figure 46 Maximum change of electrical resistance variation of sprayed EGaIn samples as a function of displacement rates

5.4.6. Comparison of Electromechanical Properties between LMEC and Sprayed EGaIn

After examining the electromechanical properties of the two materials, we took the maximum resistance variation values and consolidated them into a single graph to compare the differences between the two. Figure 45 shows the effect of strain on the maximum resistance variation for a single tensile cycle, with the red line representing the LMEC and the blue line representing Sprayed EGaIn. This graph demonstrates a significant difference in resistance variation, as the LMEC is less than 15% at 300% strain, while sprayed EGaIn is close to 75%. If we consider both materials to have a linear relationship, the slopes are 0.2057 and 0.0388, respectively. Additionally, sprayed EGaIn has already shown an exponential growth trend, indicating that as the strain continues to increase, the resistance variation will far exceed that of the LMEC.

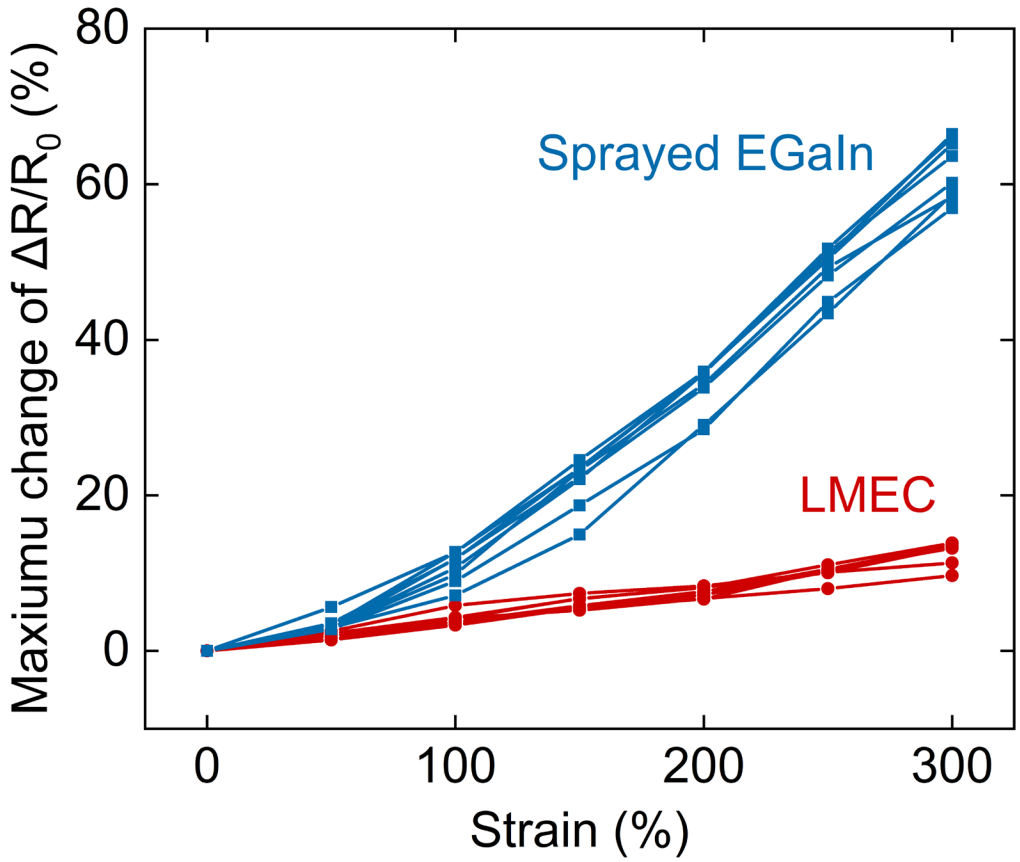

Figure 47 Maximum change of electrical resistance variation of both samples as a function of strain with different displacement rates

Figure 46 shows the effect of strain on the maximum resistance variation for five tensile cycles. While the resistance values for the two materials are significantly different, the trends are the same, with lower resistance variations at lower displacement rates. Interestingly, the lowest resistance variations for both materials were found at a displacement rate of 0.25 mm/sec.

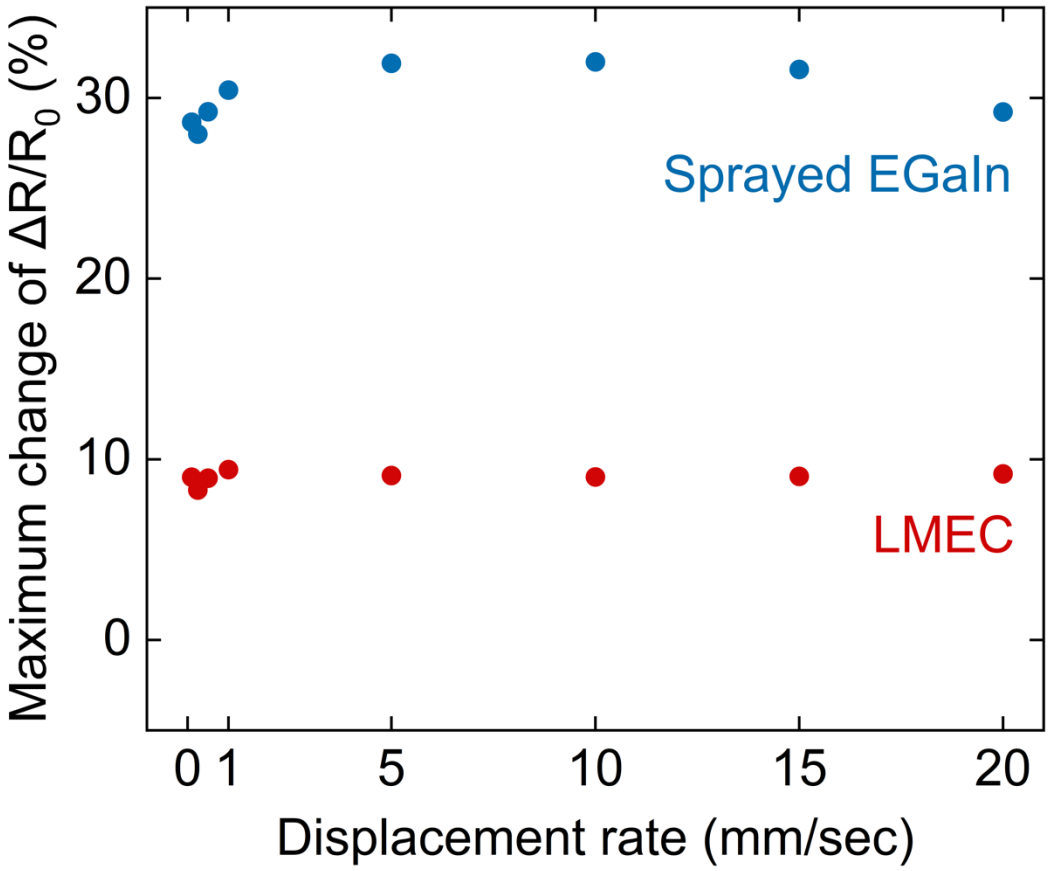

Figure 48 Maximum change of electrical resistance variation of both samples as a function of displacement rates

These comparative results demonstrate the reproducibility of this experiment, as both the LMEC and sprayed EGaIn exhibit lower resistance variations at lower displacement rates (displacement rate less than 1 mm/sec). Conversely, when the displacement rate is higher, the resistance variation will no longer change. Although this variation is not dramatic, it could have a major impact on devices that require high-precision circuits. For instance, since we now know that the resistance variation decreases to a minimum at a displacement rate of 0.25 mm/sec, devices undergoing tensile operations should not exceed this speed range to maintain optimal conductivity.

5.4.7. Electromechanical mechanisms at different displacement rates

There are two probably explanations for different resistance variation at different displacement rates.

First of all, the log-like trend observed in the curves at low displacement rates is attributed to the re-arrangement of the EGaIn particles. As the conductive pathway is stretched, its length increases while its width decreases, resulting in a natural increase in resistance due to the reduction in the

conductive cross-sectional area. However, it is challenging to ensure the complete removal of the oxide shells of all the EGaIn particles during activation, which can result in some regions being left without liquid EGaIn percolation, which is crucial for conductivity. These non-infiltrated regions can manifest to some degree in the resistance variation at high strains. When we stretch the sample at an extremely low displacement rate, it provides sufficient time for the liquid EGaIn to percolate the initially non-infiltrated regions with the strain, which can mitigate the rise in resistance variation. Therefore, we observe a saturation-like behavior with increasing strain. It can be concluded that using lower displacement rates can effectively suppress the rise of resistance variation at high strains

Secondly, this is most likely owing to the fact that stretching samples at a low displacement rate allows for the easy re-crosslinking of polymers in the LMEC and the Ecoflex substrate. This process can explain the elastomer's permanent set, which accounts for stress relaxation, the modest change in resistance at low displacement rates, and higher resistance when the samples are unloaded at low displacement rates. Because of the irreversible deformation caused by the concurrently rearranged polymer crosslinks, the cross-section of the conductive channel decreases less at these rates than at high displacement rates.

Unfortunately, we are not sure which explanation is more correct, because the displacement rate experiments are completely original. We need more investigations to study the micromechanisms and microstructures that occur in LMEC.

6. Conclusion

6.1. Reviews of the Overall Study

After much experimentation and discussion, I believe it is time to answer the three questions we asked at the beginning.

Can conductive LMEC be successfully synthesized from highly stretchable silicone elastomers with particle sizes approaching 1 micron?

After a series of tests, we confirmed that the hypothesis of "surface modification by PVP" is feasible. We first controlled the EGaIn particle size to about 1 μm by sonication at 15% power and 2 minutes 30 seconds. Then, the EGaIn particles were surface-modified using 3-4 wt.% high molecular-weight PVP. Successful surface modification of EGaIn and Ecoflex are dispersed together to form a conductive pathway through strain-activation.

Interestingly, we found that adjusting the synthesis ratios of some materials could even yield better results. For example, adjusting the ratio of Ecoflex's synthesis units A and B would not affect the samples' pure electrical conductivity but only have a poorer effect on its electromechanical properties, such as the electrical resistance variation at high strains.

Do the LM microparticles increase in size upon dispersion in an elastomer?

We attempted two methods to measure the particle size of LMEC and found that manual image analysis was more accurate. We also discovered that particle size could change during shear mixing, so we designed two particle size experiments. The results of both experiments showed that the addition of an elastic material to the sample during shear mixing could cause particle size to increase or decrease. Moreover, we observed an increase in particle size in the LMEC after shear mixing, although the change was slight (0.2 μm) and did not affect subsequent strain-activation or electromechanical properties, it is still important.

Does the electromechanical response of LM-based conductors depend on the rate of applied deformation?

We found that different displacement rates may result in different electromechanical responses during tensile testing. Therefore, we first measured the electromechanical properties of the new LMEC at different displacement rates and found that low displacement rates (rates less than 1mm/sec) had smaller resistance variation than high displacement rates. To confirm our findings,

we tested another LM-based conductor, sprayed EGaIn, under the same conditions. The results show that the low displacement rate does reduce the resistance variation, but then the high displacement rate is more stable for multi-cycle stretching. Surprisingly, the resistance variation of the new LMEC was much lower than that of sprayed EGaIn, indicating that its electromechanical properties were exceptional.

In addition, excellent measurements of electromechanical properties demonstrate the potential of this new LMEC for various applications. With a strain of up to 700% and stable/low resistance variation, it is suitable for most stretchable and wearable electronics.

6.2. Prospects for Applications and Optimization

For the prospects of this study, there are two directions that can be explored: application and optimization. In terms of application, as previously introduced, this new LMEC has many advantages. Firstly, its high degree of freedom in printability allows us to print circuits on a variety of materials with high precision, which can help expand its application scope and adapt to various uses. Secondly, it possesses high electromechanical properties, with a maximum strain of up to 700% and a resistance of only 0.2 Ω/cm, which can meet the requirements of almost all stretchable electronics. Finally, its streamlined material combination and production process, using only three readily available commercial materials, can yield excellent results, with a production time shortened to within six hours, ensuring efficiency in large-scale production.

In terms of optimization, we speculate that the method of encapsulating EGaIn particles with high-molecular weight PVP using ultrasound to weaken the solid-liquid interface may also be applicable to other polymers. If successful, this would be excellent news, as this method is both simple and effective, and can significantly reduce the production threshold of the LMEC material. Additionally, this study could also be developed in terms of particle size, as particle size directly affects the success of strain-activation. If we can organize the ultrasound coefficient's impact on particle size, it could revolutionize the development of this field.

References

1. Gu, M. *et al.* Stretchable batteries with gradient multilayer conductors. *Sci. Adv.* **5**, eaaw1879 (2019).
2. Xu, S. *et al.* Stretchable batteries with self-similar serpentine interconnects and integrated wireless recharging systems. *Nat. Commun.* **4**, 1543 (2013).
3. Yokota, T. *et al.* Ultraflexible organic photonic skin. *Sci. Adv.* **2**, e1501856 (2016).
4. Amjadi, M., Yoon, Y. J. & Park, I. Ultra-stretchable and skin-mountable strain sensors using carbon nanotubes–Ecoflex nanocomposites. *Nanotechnology* **26**, 375501 (2015).
5. Phan, H.-P. *et al.* Long-Lived, Transferred Crystalline Silicon Carbide Nanomembranes for Implantable Flexible Electronics. *ACS Nano* **13**, 11572–11581 (2019).
6. Song, E. *et al.* Thin, Transferred Layers of Silicon Dioxide and Silicon Nitride as Water and Ion Barriers for Implantable Flexible Electronic Systems. *Adv. Electron. Mater.* **3**, 1700077 (2017).
7. Park, K.-I., Jeong, C. K., Kim, N. K. & Lee, K. J. Stretchable piezoelectric nanocomposite generator. *Nano Converg.* **3**, 12 (2016).
8. Malakooti, M. H. *et al.* Liquid Metal Supercooling for Low-Temperature Thermoelectric Wearables. *Adv. Funct. Mater.* **29**, 1906098 (2019).
9. Han, Y., Simonsen, L.-E. & Malakooti, M. H. Printing Liquid Metal Elastomer Composites for High-Performance Stretchable Thermoelectric Generators. *Adv. Energy Mater.* **12**, 2201413 (2022).
10. Xu, F. & Zhu, Y. Highly Conductive and Stretchable Silver Nanowire Conductors. *Adv. Mater.* **24**, 5117–5122 (2012).
11. Tavakoli, M. *et al.* EGaIn-Assisted Room-Temperature Sintering of Silver Nanoparticles for Stretchable, Inkjet-Printed, Thin-Film Electronics. *Adv. Mater.* **30**, 1801852 (2018).

12. Tang, L.-C., Zhang, H., Sprenger, S., Ye, L. & Zhang, Z. Fracture mechanisms of epoxy-based ternary composites filled with rigid-soft particles. *Compos. Sci. Technol.* **72**, 558–565 (2012).
13. Jo, Y. *et al.* Printable Self-Activated Liquid Metal Stretchable Conductors from Polyvinylpyrrolidone-Functionalized Eutectic Gallium Indium Composites. *ACS Appl. Mater. Interfaces* **14**, 10747–10757 (2022).
14. Guan, Y. *et al.* A novel composite material for flexible wearable devices based on eutectic gallium indium (EGaIn), multi-walled carbon nanotubes (MWCNTs) and polydimethylsiloxane (PDMS). *Compos. Struct.* **291**, 115653 (2022).
15. Yan, J. *et al.* Solution processable liquid metal nanodroplets by surface-initiated atom transfer radical polymerization. *Nat. Nanotechnol.* **14**, 684–690 (2019).
16. Wei, Q. *et al.* Surface Engineering of Liquid Metal Nanodroplets by Attachable Diblock Copolymers. *ACS Nano* **14**, 9884–9893 (2020).
17. Merhebi, S. *et al.* Magnetic and Conductive Liquid Metal Gels. *ACS Appl. Mater. Interfaces* **12**, 20119–20128 (2020).
18. Wang, Q., Ji, X., Liu, X., Liu, Y. & Liang, J. Viscoelastic Metal-in-Water Emulsion Gel via Host–Guest Bridging for Printed and Strain-Activated Stretchable Electrodes. *ACS Nano* **16**, 12677–12685 (2022).
19. Houshyar, S. *et al.* Liquid metal polymer composite: Flexible, conductive, biocompatible, and antimicrobial scaffold. *J. Biomed. Mater. Res. B Appl. Biomater.* **110**, 1131–1139 (2022).

20. Kim, Y., Song, J., An, S., Shin, M. & Son, D. Soft Liquid Metal-Based Conducting Composite with Robust Electrical Durability for a Wearable Electrocardiogram Sensor. *Polymers* **14**, 3409 (2022).
21. Chen, G. *et al.* Superelastic EGaIn Composite Fibers Sustaining 500% Tensile Strain with Superior Electrical Conductivity for Wearable Electronics. *ACS Appl. Mater. Interfaces* **12**, 6112–6118 (2020).
22. Kim, J.-H., Kim, S., So, J.-H., Kim, K. & Koo, H.-J. Cytotoxicity of Gallium–Indium Liquid Metal in an Aqueous Environment. *ACS Appl. Mater. Interfaces* **10**, 17448–17454 (2018).
23. Zrnic, D. & Swatik, D. S. On the resistivity and surface tension of the eutectic alloy of gallium and indium. *J. Common Met.* **18**, 67–68 (1969).
24. Low, J.-H., Chee, P.-S., Lim, E.-H. & Ganesan, V. Design of a wireless smart insole using stretchable microfluidic sensor for gait monitoring. *Smart Mater. Struct.* **29**, 065003 (2020).
25. Koo, C. *et al.* Manipulating Liquid Metal Droplets in Microfluidic Channels With Minimized Skin Residues Toward Tunable RF Applications. *J. Microelectromechanical Syst.* **24**, 1069–1076 (2015).
26. Sun, Y.-C., Boero, G. & Brugger, J. Stretchable Conductors Fabricated by Stencil Lithography and Centrifugal Force-Assisted Patterning of Liquid Metal. *ACS Appl. Electron. Mater.* **3**, 5423–5432 (2021).
27. Hao, X. P. *et al.* Self-Shaping Soft Electronics Based on Patterned Hydrogel with Stencil-Printed Liquid Metal. *Adv. Funct. Mater.* **31**, 2105481 (2021).
28. Boley, J. W., White, E. L. & Kramer, R. K. Mechanically sintered gallium-indium nanoparticles. *Adv. Mater. Deerfield Beach Fla* **27**, 2355–2360 (2015).

29. Lin, Y. *et al.* Handwritten, Soft Circuit Boards and Antennas Using Liquid Metal Nanoparticles. *Small* **11**, 6397–6403 (2015).
30. Tang, L., Mou, L., Zhang, W. & Jiang, X. Large-Scale Fabrication of Highly Elastic Conductors on a Broad Range of Surfaces. *ACS Appl. Mater. Interfaces* **11**, 7138–7147 (2019).
31. Ren, L. *et al.* Nanodroplets for Stretchable Superconducting Circuits. *Adv. Funct. Mater.* **26**, 8111–8118 (2016).
32. Vallem, V., Aggarwal, V. & Dickey, M. D. Stretchable Liquid Metal Films with High Surface Area and Strain Invariant Resistance. *Adv. Mater. Technol.* **8**, 2201233 (2023).
33. Farrell, Z. J., Thrasher, C. J., Flynn, A. E. & Tabor, C. E. Silanized Liquid-Metal Nanoparticles for Responsive Electronics. *ACS Appl. Nano Mater.* **3**, 6297–6303 (2020).
34. Goh, Q.-L., Chee, P.-S., Lim, E.-H. & Ng, D. W.-K. An AI-Assisted and Self-Powered Smart Robotic Gripper Based on Eco-EGaIn Nanocomposite for Pick-and-Place Operation. *Nanomaterials* **12**, 1317 (2022).
35. Banerjee, S. S. *et al.* Designing Supertough and Ultrastretchable Liquid Metal-Embedded Natural Rubber Composites for Soft-Matter Engineering. *ACS Appl. Mater. Interfaces* **13**, 15610–15620 (2021).
36. Yun, G. *et al.* Liquid Metal Hybrid Composites with High-Sensitivity and Large Dynamic Range Enabled by Micro- and Macrostructure Engineering. *ACS Appl. Polym. Mater.* **3**, 5302–5315 (2021).
37. Darby, D. R., Cai, Z., Mason, C. R. & Pham, J. T. Modulus and adhesion of Sylgard 184, Solaris, and Ecoflex 00-30 silicone elastomers with varied mixing ratios. *J. Appl. Polym. Sci.* **139**, e52412 (2022).

38. Liu, Y. *et al.* Water Processable Liquid Metal Nanoparticles by Single Step Polymer Encapsulation. *Nanoscale* **12**, (2020).
39. Piwek, L., Ellis, D. A., Andrews, S. & Joinson, A. The Rise of Consumer Health Wearables: Promises and Barriers. *PLOS Med.* **13**, e1001953 (2016).
40. Wu, W. Stretchable electronics: functional materials, fabrication strategies and applications. *Sci. Technol. Adv. Mater.* **20**, 187–224 (2019).
41. Hajalilou, A. *et al.* Biphasic Liquid Metal Composites for Sinter-Free Printed Stretchable Electronics. *Adv. Mater. Interfaces* **9**, 2101913 (2022).
42. Guymon, G. G. & Malakooti, M. H. Multifunctional liquid metal polymer composites. *J. Polym. Sci.* **60**, 1300–1327 (2022).
43. Chiew, C., Morris, M. J. & Malakooti, M. H. Functional liquid metal nanoparticles: synthesis and applications. *Mater. Adv.* **2**, 7799–7819 (2021).
44. Malakooti, M. H., Bockstaller, M. R., Matyjaszewski, K. & Majidi, C. Liquid metal nanocomposites. *Nanoscale Adv.* **2**, 2668–2677 (2020).
45. Chen, S., Wang, H.-Z., Zhao, R.-Q., Rao, W. & Liu, J. Liquid Metal Composites. *Matter* **2**, 1446–1480 (2020).
46. Park, J.-E. *et al.* Rewritable, Printable Conducting Liquid Metal Hydrogel. *ACS Nano* **13**, 9122–9130 (2019).
47. Crater, E. R., Tutika, R., Moore, R. B. & Bartlett, M. D. X-ray scattering as an effective tool for characterizing liquid metal composite morphology. *Soft Matter* **18**, 7762–7772 (2022).